Efficient Detection of ^{1}H, ^{15}N Correlations in Hydrogen Bonded Low Molecular Catalyst-Substrate Intermediates without Selective ^{15}N Labelling

Christian L. Scholtes, Julian Ilgen and Ruth M. Gschwind*

Institut für Organische Chemie,

Universität Regensburg, D-93053 Regensburg, Germany

Email: ruth.gschwind@ur.de

Supporting Information

Table of Content

S1 Experimental Data

S1.1 Chemicals

DCM-d_2 was purchased from Deutero. For this study anhydrous DCM-d_2 was distilled over CaH_2 under argon and further dried over activated 3 Å molecular sieves for at least 3 d. The chiral phosphoric acids were purchased from abcr. The tetrafluoroboric acid diethyl ether complex was purchased from Sigma Aldrich.

S1.2 Synthesis of the Imines

The imines **1a**, **1b** and **1c** are already described in literature[S1] and were synthesized by refluxing aniline and the corresponding ketone over activated 4 Å molecular sieves in toluene according to a modified literature procedure. Toluene was used in p.A. quality. N.B. Using toluene from a solvent purifying system (SPS) and working under dry conditions did not result in a reaction. Adding a drop of water help to start the reaction.

1-(4 methoxyphenyl)-*N*-phenylethan-1-imine (1a)

The following procedure of the synthesis serves as exemplary description on how the other imines were synthesized.

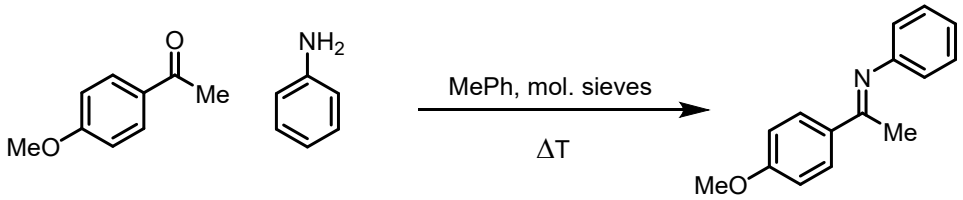

4-methoxyacetophenone (900 mg, 6 mmol) were weighed into a round flask. Some activated 4 Å molecular sieves, toluene (20 mL) and aniline (0.6 mL, 6.6 mmol) were added to the round flask. The flask was equipped with a reflux condenser. The solution was heated to reflux overnight. The orange solution was filtered off from the molecular sieves and was concentrated under reduced pressure. The remaining oil solidified over night in the fridge. If this was not the case, the some of the remaining ketone was distilled from the oil to facilitate the solidification. The obtained solid was recrystallized from diethyl ether. The product was obtained as light yellow solid (0.227 g, 1.8 mmol, 30 %) and predominantly as *E*-isomer (>99 % via ^{1}H-NMR analysis). The spectrum reference frequency (SR) was set to 0 Hz.

^{1}H-NMR (400.13 MHz, CD_2Cl_2) δ/ppm = 7.98 (m, 2H, Aryl-H), 7.37 (m, 2H, Aryl-H), 7.10 (m, 1H, Aryl-H), 6.99 (m, 2H, Aryl-H), 6.79 (m, 2H, Aryl-H), 3.90 (s, 3H, -OMe), 2.22 (s, 3H, -Me)

1-(4-methylphenyl)-*N*-phenylethan-1-imine (1b)

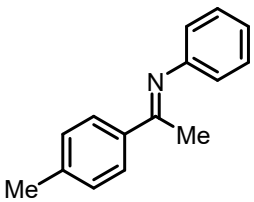

The synthesis was executed as described for imine **1a**. The SR was set to 0 Hz.

^{1}H-NMR (400.13 MHz, CD_2Cl_2) δ/ppm = 7.91 (d, $^3J_{HH}$ = 8.12 Hz, 2H, Aryl-H), 7.38 (m, 2H, Aryl-H), 7.30 (d, $^3J_{HH}$ = 8.12 Hz, 2H, Aryl-H), 7.11 (m, 1H, Aryl), 6.80 (m, 2H), 2.45 (s, 3H, -Me) 2.23 ppm (s, 3H, -Me)

1-(4-(trifluoromethyl)phenyl)-*N*-phenylethan-1-imine (1c)

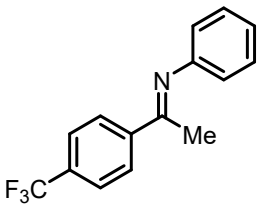

The synthesis was executed as described for imine **1a**. The SR was set to 0 Hz.

^{1}H-NMR (400.13 MHz, CD_2Cl_2) δ/ppm = 8.15 (m, 2H, Aryl-H), 7.76 (m, 2H, Aryl-H), 7.41 (m, 2H, Aryl-H), 7.15 (m, 1H, Aryl-H), 6.83 (m, 2H, Aryl-H), 2.28 ppm (s, 3H, -Me)

^{19}F-NMR (376.50 MHz, CD_2Cl_2) δ/ppm = -63.1

S1.3 Sample Preparation of Binary Complexes in DCM-d_2

The chiral phosphoric acids (CPAs) were directly weighed into a 5 mm NMR tube and dried for 90 min at 150 °C under reduced pressure. Imines were weighted onto a weighing paper and transferred into the NMR tube. Before adding 0.5 mL of anhydrous DCM-d_2, the NMR tube was put under inert gas argon atmosphere. For the samples with HBF_4, imine and DCM-d_2 were first transferred into an NMR tube under inert gas argon atmosphere. Only at the end were 3.4 µL of HBF_4 added to the prepared sample.For all samples a 1:1 ratio of acid/ketimine wasused. A concentration of 50 mM was used for all samples. These conditions have been chosen to reduce the line widths of our hydrogen bond signals, which is significantly broadened if exchange processes are present. The structural motif of the intermediate is not affected by the 1:1 ratio of imine to CPA, since the stereoselective reaction outcome is not affected. Even after careful sample preparation, partial hydrolysis of the imine could not beprevented. Therefore, the imine/acid ratios are slightly different from 1:1 and leading to the fact that ketone is always visible in the spectra.

S2 Spectroscopical Data

S2.1 NMR Spectroscopy

NMR experiments were performed on Bruker Avance III HD spectrometer operating at a ^{1}H base frequency of 600.03 MHz equipped either with a 5 mm triple resonance broadband inverse probe TBI-F (^{1}H/^{19}F, BB, ^{2}H) with z-gradient (56 G·cm^{-1}) or a 5 mm triple resonance broadband observe probe TBO-N (BB, ^{1}H/^{15}N, ^{2}H) (TBO-N) with z-gradient (51 G·cm^{-1}). Temperature regulation at 180 K was performed using a N_2 evaporator. The sample temperature was checked with a methanol-d_4 (99.8% deuteration) sample applying the calibration model reported by Karschin et al.[S2] Spectrometers were operated with TopSpin (version 3.5 PL2, Bruker BioSpin, 2017). NMR data were processed and plotted with TopSpin 3.2 PL 7 software. Further plotting of the spectra was performed with Corel Draw 2022 software.

Routine NMR experiments to certify the quality of the used chemicals were performed on Bruker Avance III HD operating at a ^{1}H base frequency of 400.13 MHz equipped with a 5 mm broadband observe probe BBFO (BB/^{19}F, ^{1}H, ^{2}H) with z-gradient.

S2.2 Pulse Programmes

Unless reported otherwise, measurements were performed using 1D and 2D experiments available in the Bruker pulse sequence library such as 1D ^{1}H (*zg*, *zg30*), 1D ^{13}C (*zgpg30*), 1D ^{1}H-Inversion-recovery (*t1ir1d*), 1D ^{1}H pulsed-field gradient-selected selective spin-echo (*selgpse*), 2D ^{1}H-NOESY (*noesygpphzs*) and 2D ^{1}H-EASY-ROESY (*roesyadjsph*).

The ^{1}H, ^{15}N-SOFAST-HMQC (*sfhmqcf3gpph*) experiment from the Bruker pulse sequence library has been modified to adjust the excitation angle (CNST8) of the selective PC9 pulse. Furthermore, a modified IPAP-SOFAST-HMQC pulse sequence developed by Paul Schanda for the determination of $^{1}J_{HN}$-coupling constants has been used, which is referred to as *sfhmqcipjc* in the following.

For reasons of comparability between inversion recovery experiments in fully deuterated DCM-d_2 (99.5 %) and 10 % deuterated DCM, the solvent peak has been suppressed by implementing excitation sculpting with gradients into the Bruker sequence *t1ir1d*. For this reason, in the following, it will be referred to as *t1iresgp*. For the selective inversion recovery experiments (*selt1ir1desgp*), both inversion and excitation broadband pulses of the *t1ir1desgp* have been changed to selective pulses.

For the acquisition of the sensitivity enhancement curves, two pulse sequences have been used. First, the reference data sets are collected with the 1D ^{1}H pulsed-field gradient-selected selective spin-echo (*selgpse*). The selective echo experiment has been used instead of the standard 1D ^{1}H to ensure in all experiments the same receiver gain value (RG) without the risk of a receiver overflow and for proper intensity comparisons. Herein the offset of the selective refocusing pulse was set to the chemical shift region of the hydrogen bond protons. Second, for the sensitivity enhancement curves, an 1D ^{1}H version of the SOFAST-HMQC pulse sequence with removed ^{15}N-filtering has been used (*sofast1d*).

S2.3 Acquisition Parameters

^{1}H, ^{15}N-SOFAST-HMQC	PULPROG = sfhmqcf3gpph, D1 = 0.11-0.125 s, AQ = 57-228 ms, (2 SW, 1 SW) = (30 ppm, 10-30 ppm), (2 TD, 1 TD) = (2048, 32-64), NS = 256-1024, DS = 16, O1P = 15.83--18.2 ppm, O3P = 188-231.5 ppm, P39 = 2400 µs, P40 = 2000 µs, CNST4 = 71-93 Hz, CNST8 = 120°, SP23 = Pc9_4_120.1000, SP24 = Reburp.1000.
^{1}H, ^{31}P-SOFAST-HMBC	PULPROG = sfhmbc, D1 = 0.05 s, AQ = 114 ms, (2 SW, 1 SW) = (30 ppm, 10 ppm), (2 TD, 1 TD) = (4096, 32), NS = 256, DS = 16, O1P = 15.79 ppm, O2P = 2.85 ppm, P39 =1942.8 µs, P40 = 2000 µs, CNST8 = 120°, CNST13 = 50 Hz, SP23 = Pc9_4_120.1000, SP24 = Reburp.1000.
^{1}H, ^{15}N-CLIP-SOFAST-HMQC as 1D	PULPROG = sfhmqcipjc, D1 = 0.125 s, AQ = 114-228 ms, SW = 30 ppm, TD = 2048-4096, NS = 4096-32768, DS = 16, O1P = 15.7-16.25 ppm, O3P = 204-206 ppm, P39 =2400µs, P40 = 2000 µs, CNST4 = 82-83 Hz, CNST8 = 120°, SP23 = Pc9_4_120.1000, SP24 = Reburp.1000.
^{1}H, ^{15}N-CLIP-SOFAST-HMQC as 2D	PULPROG = sfhmqcipjc, D1 = 0.125 s, AQ = 114-228 ms, (2 SW, 1 SW) = (30 ppm, 4.5-11 ppm), (2 TD, 1 TD) = (2048-4096, 32-64), NS = 1024-2048, DS = 16, O1P = 12.68-17.28 ppm, O3P = 185-231.5 ppm, P39 =2400 µs, P40 = 2000 µs, CNST4 = 71-93 Hz, CNST8 = 120°, SP23 = Pc9_4_120.1000, SP24 = Reburp.1000.
^{1}H-NOESY	PULPROG = noesygpphzs, D1 = 1.5 s, AQ = 228 ms, (2 SW, 1 SW) = (15 ppm, 15 ppm), (2 TD, 1 TD) = (4096, 512), NS = 16, DS = 16, O1P = O3P =9.5, P32 =40 ms, D8 = 150 ms, SPNAM29 = Crp30,40,10.10000.
^{1}H-ROESY	PULPROG = roesyadjsph, D1 = 1.5 s, AQ = 228 ms, (2 SW, 1 SW) = (15 ppm, 15 ppm), (2 TD, 1 TD) = (4096, 512), NS = 16, DS = 16, O1P = O3P =9.5, P15 = 150 ms, CNST26 =5000, CNST28=45
Broadband inversion recovery	PULPROG = t1ir1desgp, D1 =13 s, AQ = 1.82 s, SW = 30 ppm, TD = 65536, NS = 8, DS = 4, O1P = 7.57, D7 = 25 us-25 s.
Selective inversion recovery	PULPROG = selt1ir1desgp, D1 = 13 s, AQ = 1.82 s, SW = 30 ppm, TD = 65536, NS = 16-32, DS = 4, O1P = 15.84 ppm, D7 = 25 us- 20 s.
Sensitivity enhancement, reference	PULPROG = selgpse, D1 = 30 ms-1.97 s, AQ = 57 ms, SW = 30 ppm, TD = 2048, NS = 16-512, DS = 16, O1P = 15.83 ppm, SPNAM2 = ReBurp.1000, P12 = 2m.
Sensitivity enhancement	PULPROG = sofast1d, D1 = 30 ms-1.97 s, AQ = 57 ms, SW = 30 ppm, TD = 2048, NS = 16-512, DS = 16, O1P = 15.83 ppm, P39 = 2400 µs, P40 = 2000 µs, CNST8 = 90-140°, SP23 = Pc9_4_120.1000, SP24 = Reburp.1000.

In the case of the SOFAST experiments, important parameters such as NS, TD, AQ, O1P/ppm, O2P/ppm or O3P/ppm and CNST4/Hz ($^{1h}J_{NH}$) or CNST13/Hz ($^{2h}J_{PH}$) are specified below the corresponding spectrum. Additionally, the total acquisition time is specified.

Routine NMR experiments

^{1}H-NMR	PULPROG = zg30, D1 = 2 s, AQ = 2.72 s, SW = 30 ppm, TD = 65536, NS = 16, DS = 2

S3 SOFAST Pulse Sequences

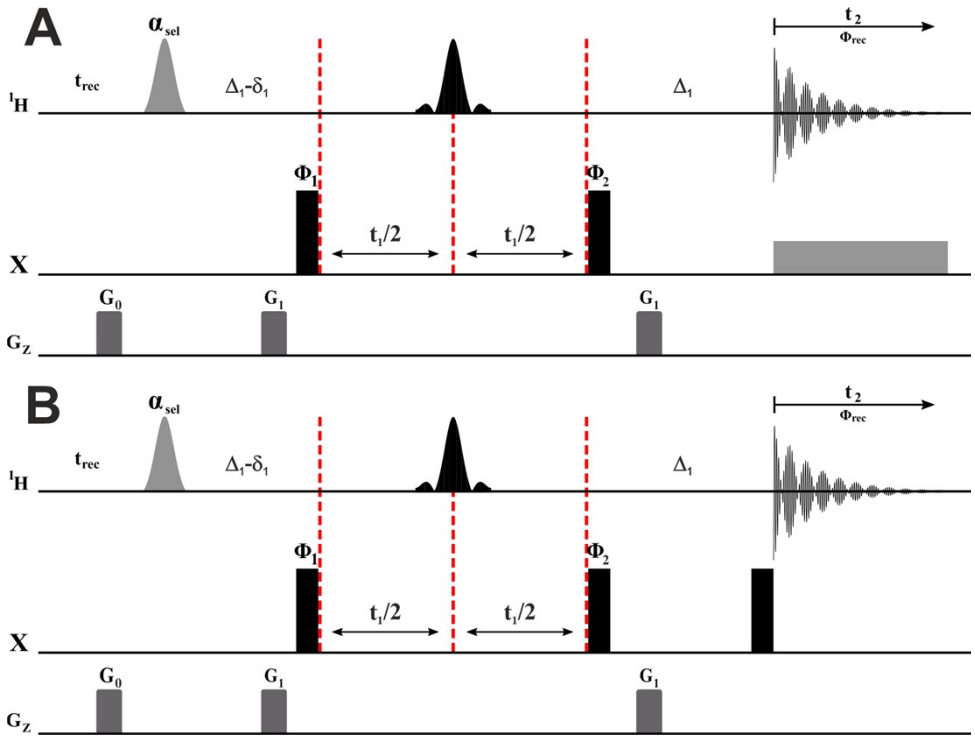

Figure S1: Pulse sequence schemes for **A** the ^{1}H, X-SOFAST-HMQC experiment[S3] and **B** the ^{1}H, X-CLIP-SOFAST-HMQC.[S4] Narrow black rectangles represent broadband 90° pulses. The broad rectangle in grey in **A** represents the composite pulse decoupling during acquisition (garp4).[S5] Gaussian grey and black shapes are selective pulses with variable flip-angle α (90°-140°, PC9) and 180° (ReBurp),[S6] respectively. The gradient G_0 represents a purge gradient to diphase residual transversal magnetization. The gradients G_1 are used for coherence selection. The delay Δ_1 is set to $1/2^{1}J_{HX}$, whereas the delay δ_1 compensates for the chemical shift and *J*-coupling evolution during the PC9-excitation pulse.[S7] Quadrature detection in the indirect dimension is implemented using the States-TPPI protocol,[S8] whereby the phase ϕ_1 is incremented. Phase cycling: All pulse phases are x unless other denoted. ϕ_1 = x, –x, ϕ_2 =x, x, –x, –x, and ϕ_{rec} = x, –x, –x, x.

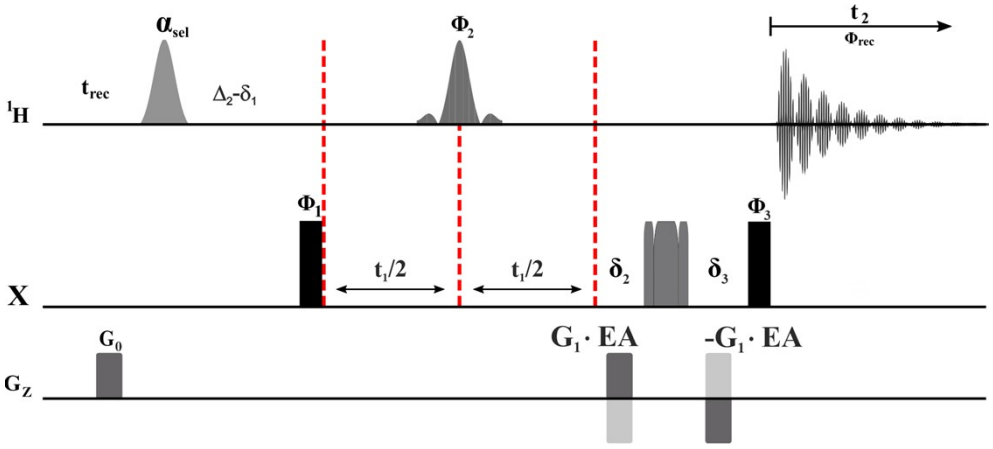

Figure S2: Pulse sequence scheme for the ^{1}H, X-SOFAST-HMBC experiment.[S9] Narrow black rectangles represent broadband 90° pulses. Gaussian grey and black shapes are selective pulses with variable flip-angle α (90°-140°, PC9) and 180° (ReBurp), respectively. The grey triple-gaussian shape represents an adiabatic broadband, composite refocusing pulse. The gradient G_0 represents a purge gradient to diphase residual transversal magnetization. The gradients G_1, weighted with the gyromagnetic ration γ of ^{1}H and X, are used for selection of double and zero quantum coherences. The delay Δ_2 is set to $1/2^{n}J_{HX}$, whereas the delay δ_1 compensates for the chemical shift and *J*-coupling evolution during the PC9-excitation pulse.[S7] Quadrature detection in the indirect dimension is implemented using the Echo-Antiecho (EA) protocol,[S10] whereby the gradients are inverted every second increment as well as the phases ϕ_1 and ϕ_{rec} are incremented together with t_1 incrementation. Phase cycling: All pulse phases are x unless other denoted. ϕ_1 = x, –x, ϕ_2 =x, x, –x, –x, ϕ_3 =4(x), 4(–x), and ϕ_{rec} = 2(x, –x), 2(–x, x).

S4 SOFAST-HMQC Spectra and Parameters

S4.1 Binary Complexes of imines formed with acid 2a (TRIFP)

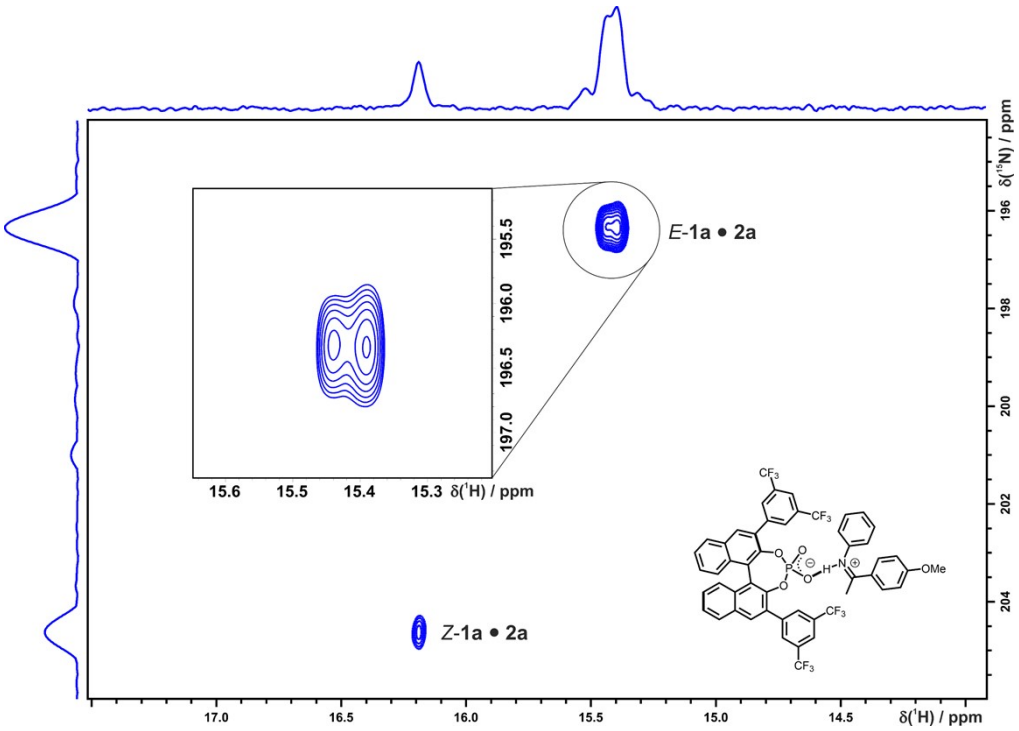

Figure S3: Low field section of the ^{1}H, ^{15}N-SOFAST-HMQC with ^{15}N broadband decoupling acquired for **1a•2a** at 180 K. Further information: NS = 512, (2 TD, 1 TD) = (2048, 48), AQ = 57 ms, O1P = 15.83, O3P = 200, CNST4 = 85. Acquired in 91 min. The observed splitting of the *E*-**1a•2a** can be assigned to a large $^{2h}J_{PH}$ coupling. Whether the $^{2h}J_{PH}$ is observed depends on its size and the spectral resolution.

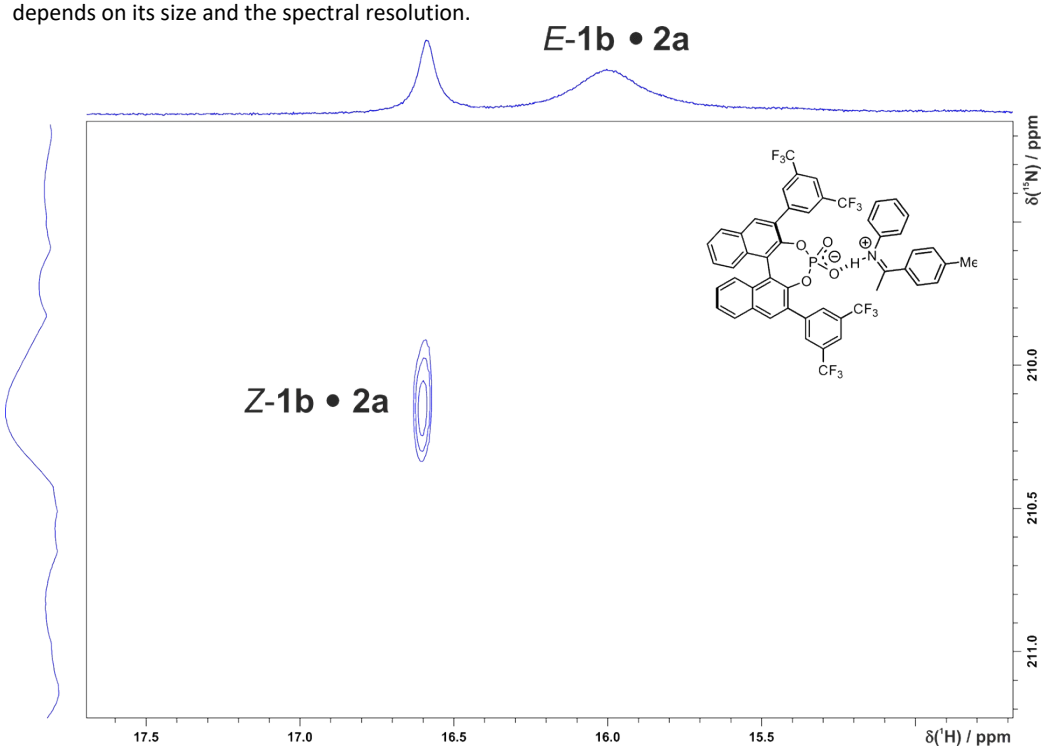

Figure S4 Low field section of the ^{1}H, ^{15}N-SOFAST-HMQC acquired for **1b•2a** at 180 K. Further information: NS = 512, (2 TD, 1 TD) = (2048, 32), AQ = 57 ms, O1P = 16.25, O3P = 207, CNST4 = 84. Acquired in 66 min. The *E*-complex is not detectable due to exchange processes.

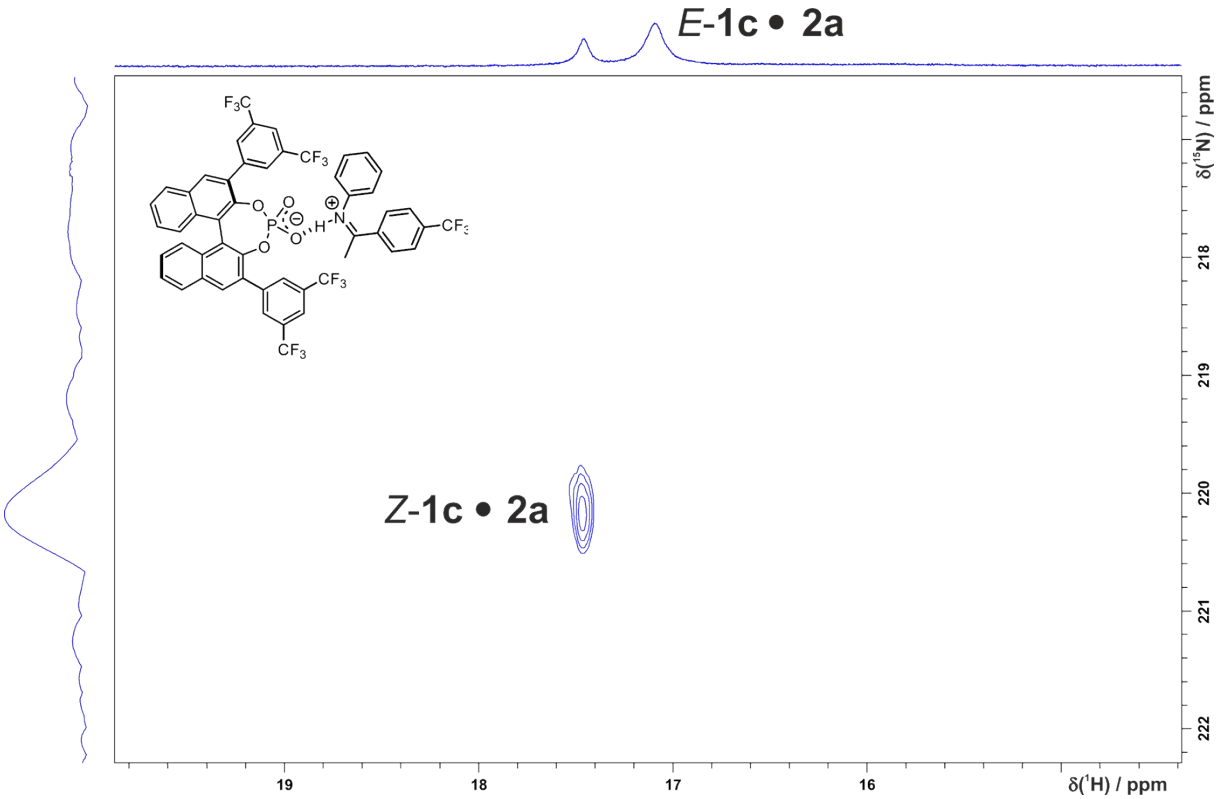

Figure S5: Low field section of the ^{1}H, ^{15}N-SOFAST-HMQC acquired for **1c•2a** at 180 K. Further information: NS = 1024, (2 TD, 1 TD) = (2048, 32), AQ = 57 ms, O1P = 17.28, O3P = 219, CNST4 = 81. Acquired in 124 min. The *E*-complex is not detectable due to exchange processes.

S4.2 Binary Complexes of imines formed with acid 2b (TRIP)

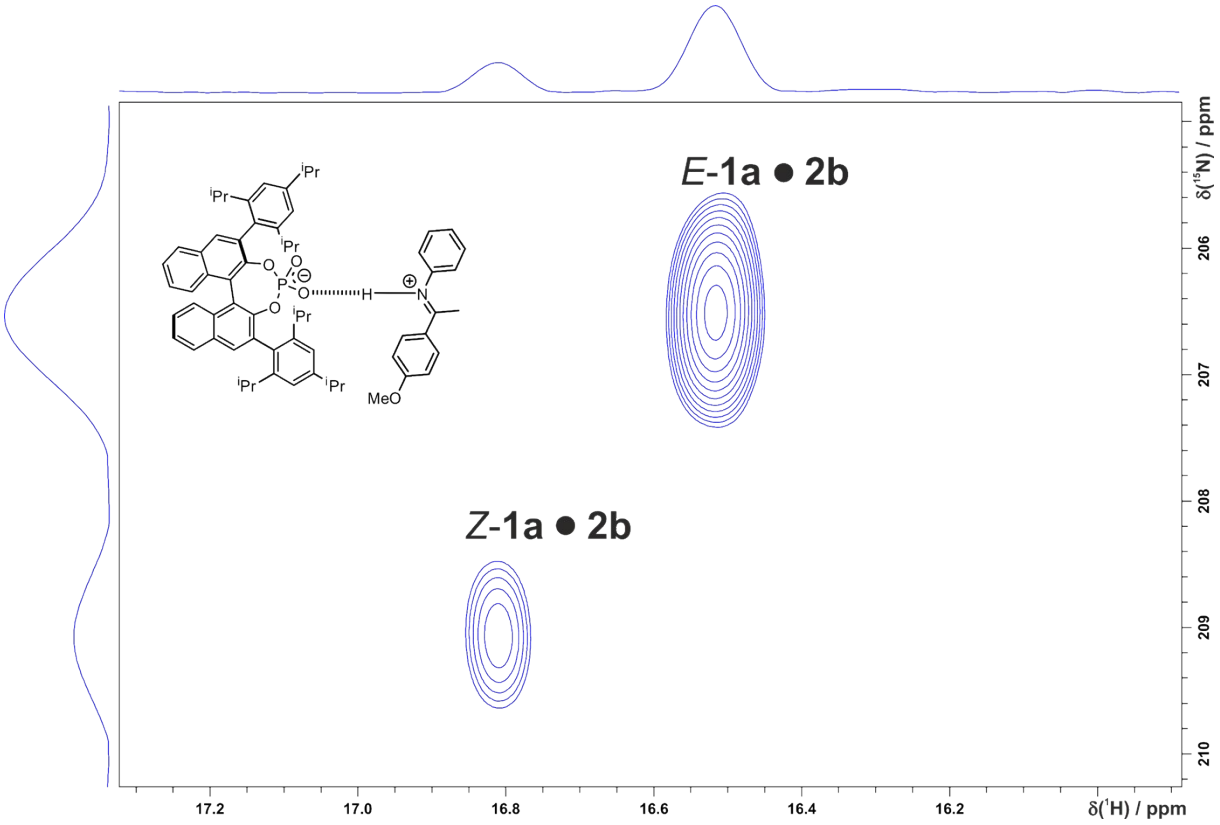

Figure S6: Low field section of the ^{1}H, ^{15}N-SOFAST-HMQC acquired for **1a•2b** at 180 K. Further information: NS = 512, (2 TD, 1 TD) = (2048, 48), AQ = 57 ms, O1P = 16.68, O3P = 207.5, CNST4 = 82. Acquired in 97 min.

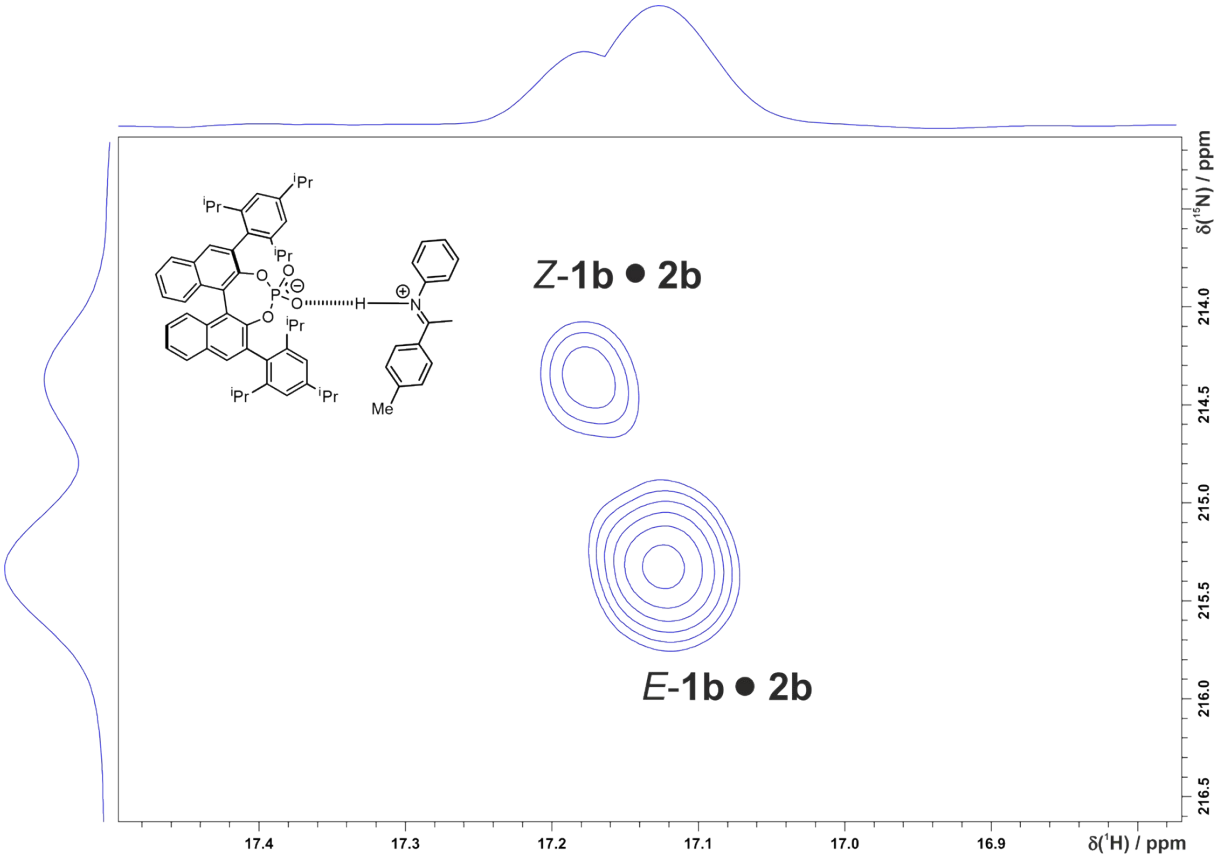

Figure S7: Low field section of the ^{1}H, ^{15}N-SOFAST-HMQC acquired for **1b•2b** at 180 K. Further information: NS = 512, (2 TD, 1 TD) = (2048, 48), AQ = 57 ms, O1P = 17.15, O3P = 215.5, CNST4 = 79. Acquired in 97 min.

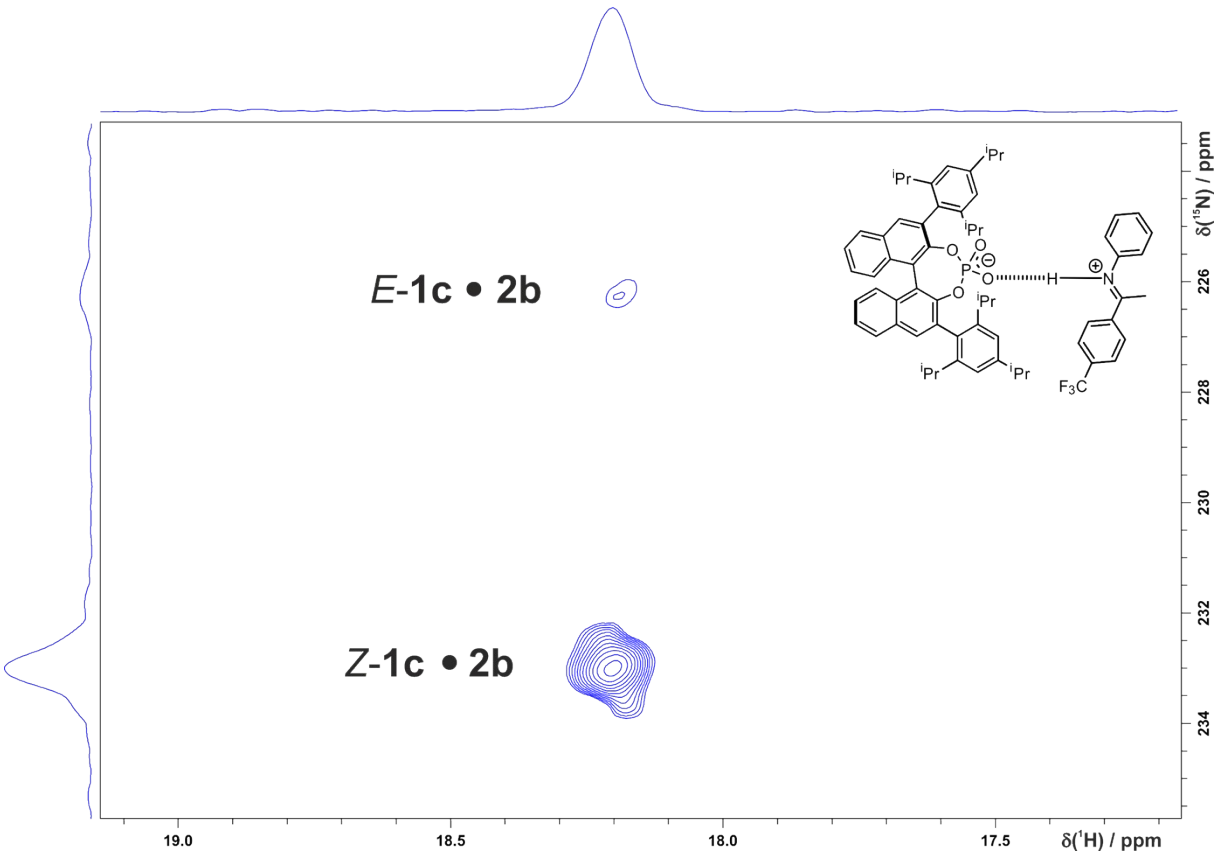

Figure S8: Low field section of the ^{1}H, ^{15}N-SOFAST-HMQC acquired for **1c•2b** at 180 K. Further information: NS = 512, (2 TD, 1 TD) = (2048, 48), AQ = 57 ms, O1P = 18.20, O3P = 231.5, CNST4 = 71. Acquired in 97 min.

S4.3 Binary Complexes of imines formed with acid 3 (HBF_4)

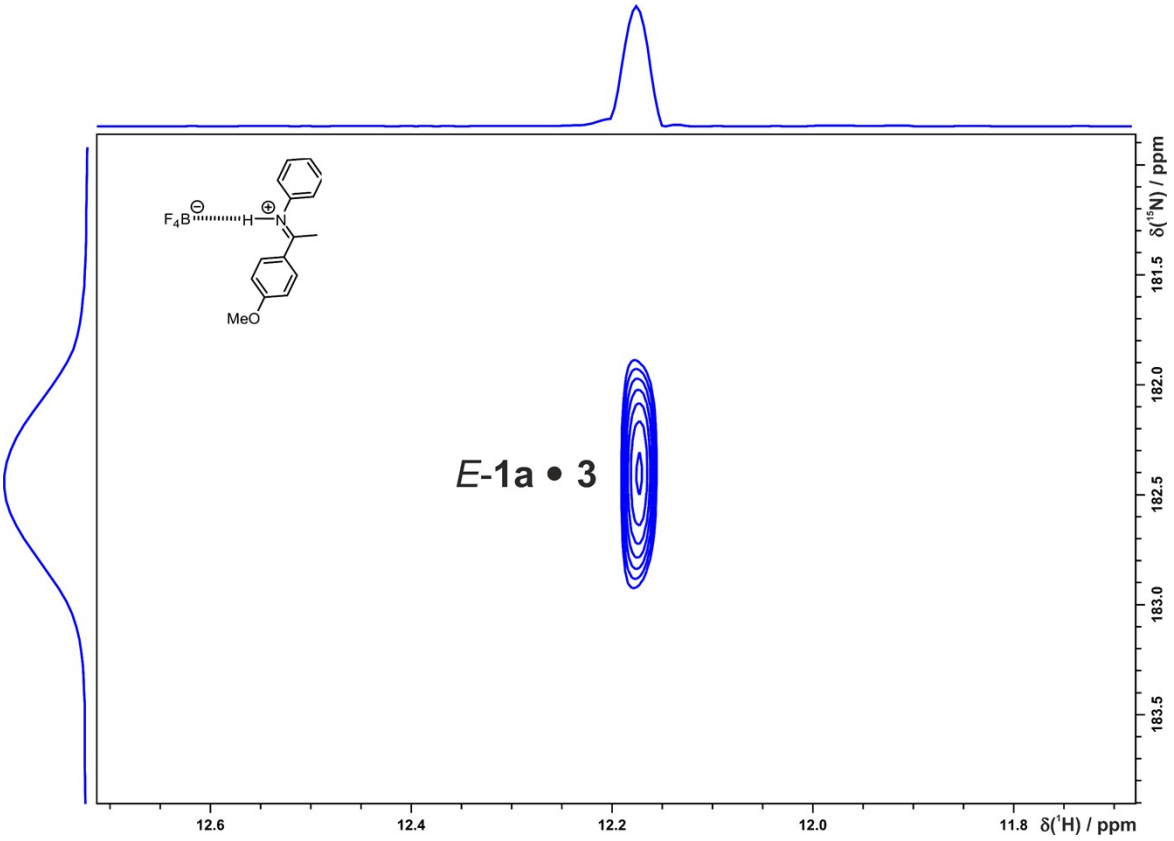

Figure S9: Low field section of the ^{1}H, ^{15}N-SOFAST-HMQC acquired for **1a•3** at 180 K. Further information: NS = 512, (2 TD, 1 TD) = (2048, 64), AQ = 57 ms, O1P = 18.20, O3P = 231.5, CNST4 = 93. Acquired in 167 min.

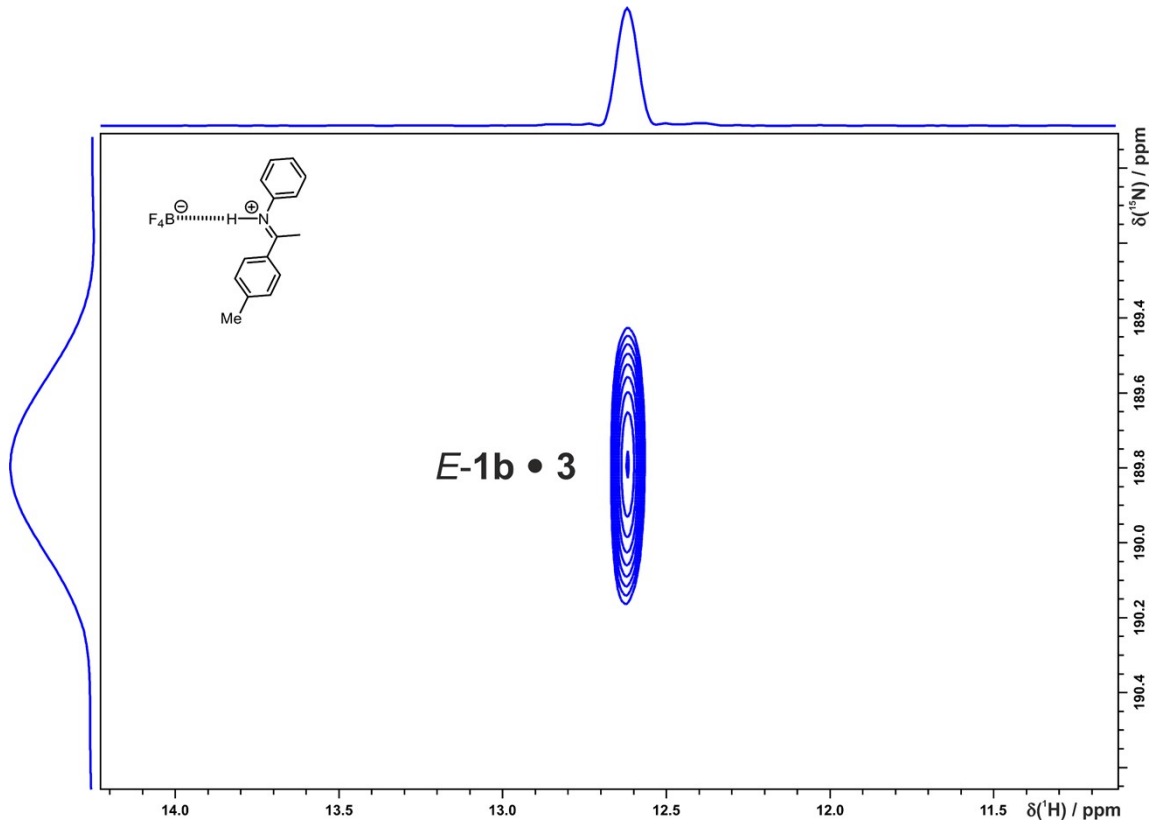

Figure S10: Low field section of the ^{1}H, ^{15}N-SOFAST-HMQC acquired for **1b•3** at 180 K. Further information: NS = 1024, (2 TD, 1 TD) = (2048, 32), AQ = 57 ms, O1P = 12.68, O3P = 191.4, CNST4 = 92. Acquired in 259 min.

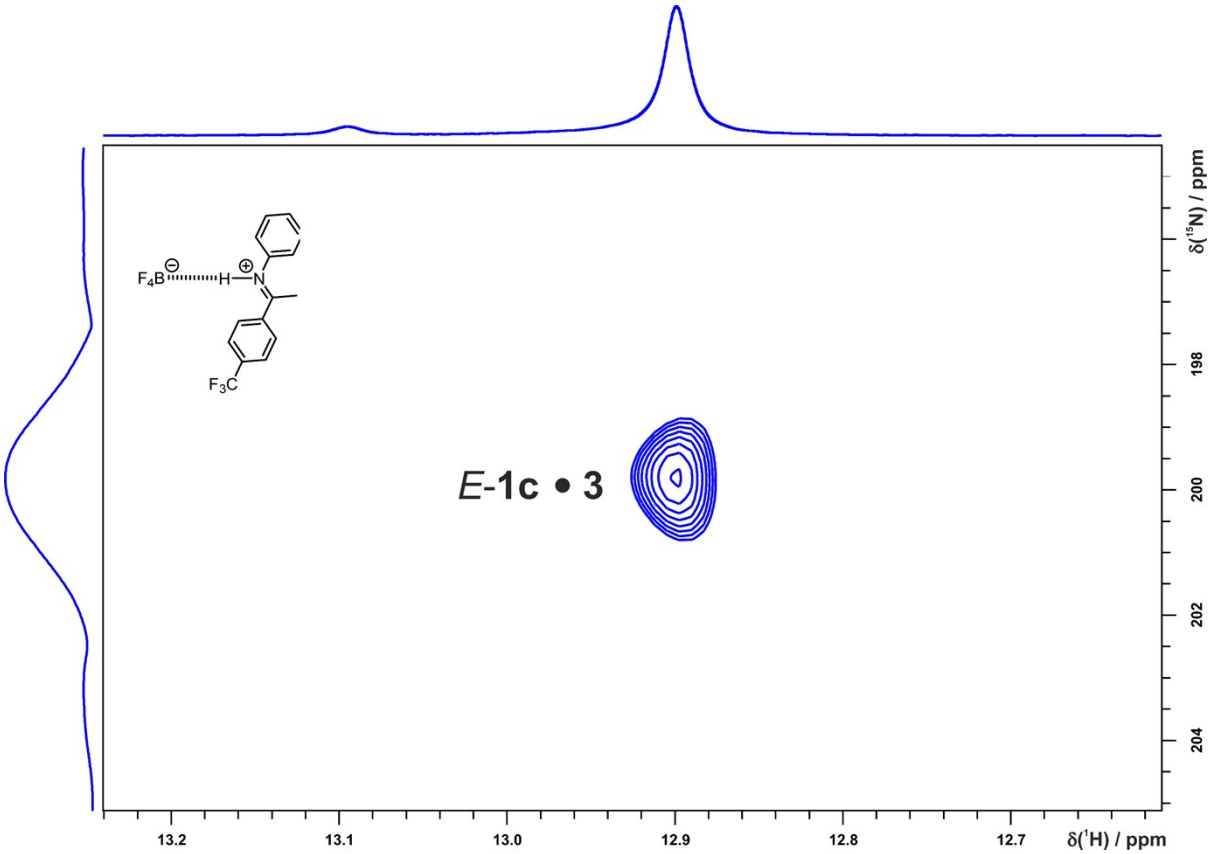

Figure S11: Low field section of the ^{1}H, ^{15}N-SOFAST-HMQC acquired for **1c•3** at 180 K. Further information: NS = 64, (2 TD, 1 TD) = (4096, 64), AQ = 114 ms, O1P = 13.00, O3P = 183.00, CNST4 = 92. Acquired in 19 min.

S5 SOFAST-CLIP-HMQC Spectra and Parameters

S5.1 Binary Complexes of imines formed with acid 2a (TRIFP)

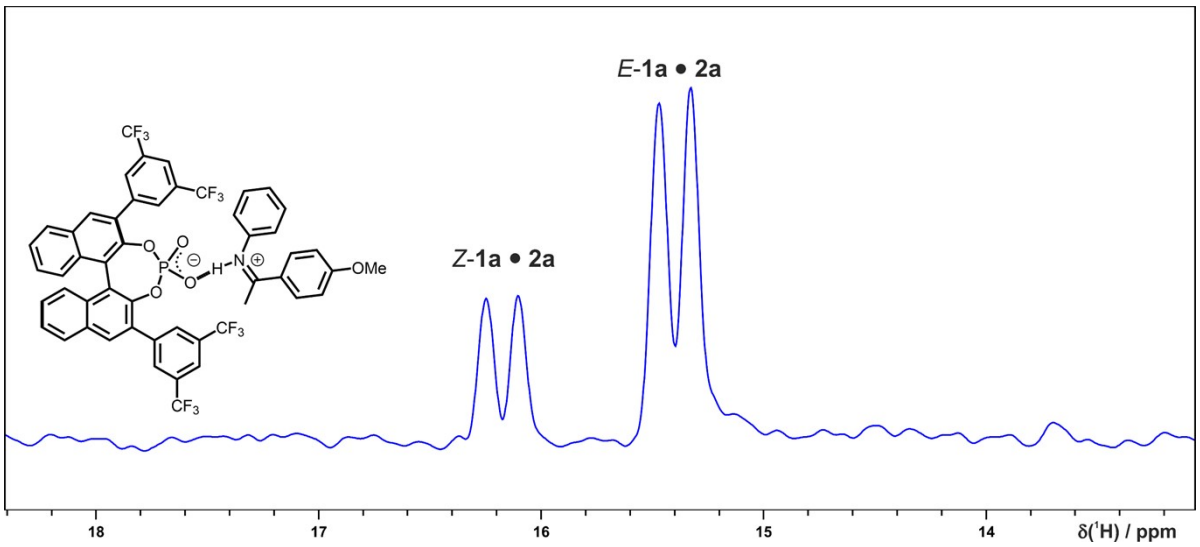

Figure S12: Low field section of the ^{1}H, ^{15}N-SOFAST-CLIP-HMQC acquired for **1a•2a** at 180 K. Further information: NS = 4096, TD = 4096, AQ = 114 ms, O1P = 15.8, O3P = 200, CNST4 = 85.5. Acquired in 16 min.

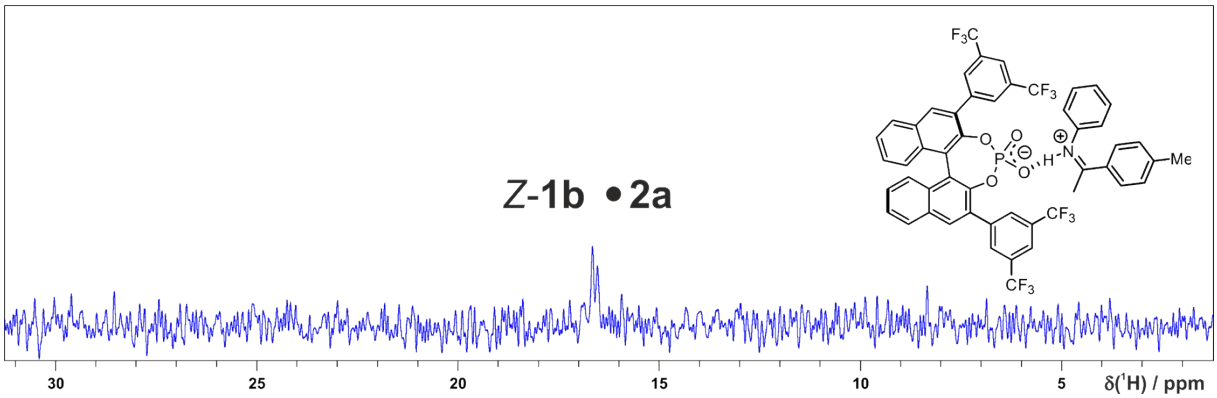

Figure S13: Low field section of the ^{1}H, ^{15}N-SOFAST-CLIP-HMQC acquired for **1b•2a** at 180 K. Further information: NS = 32048, TD = 2048, AQ = 114 ms, O1P = 16.25, O3P =215, CNST4 = 83. Acquired in 126 min. The *E*-complex is not detectable due to exchange processes.

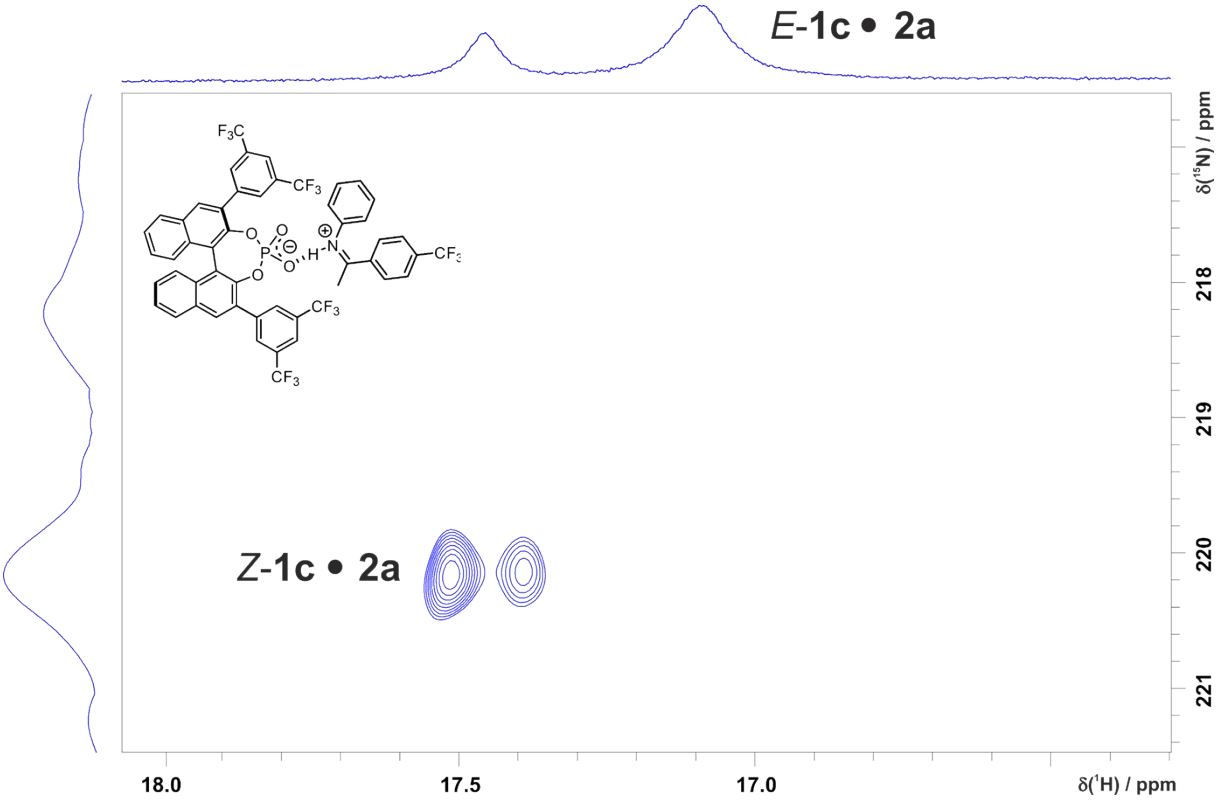

Figure S14: Low field section of the ^{1}H, ^{15}N-SOFAST-CLIP-HMQC acquired for **1c•2a** at 180 K. Further information: NS = 4096, (2 TD, 1 TD) = (2048, 16), AQ = 57 ms, O1P = 17.28, O3P = 219, CNST4 = 81. Acquired in 264 min. The *E*-complex is not detectable due to exchange processes.

S5.2 Binary Complexes of imines formed with acid 2b (TRIP)

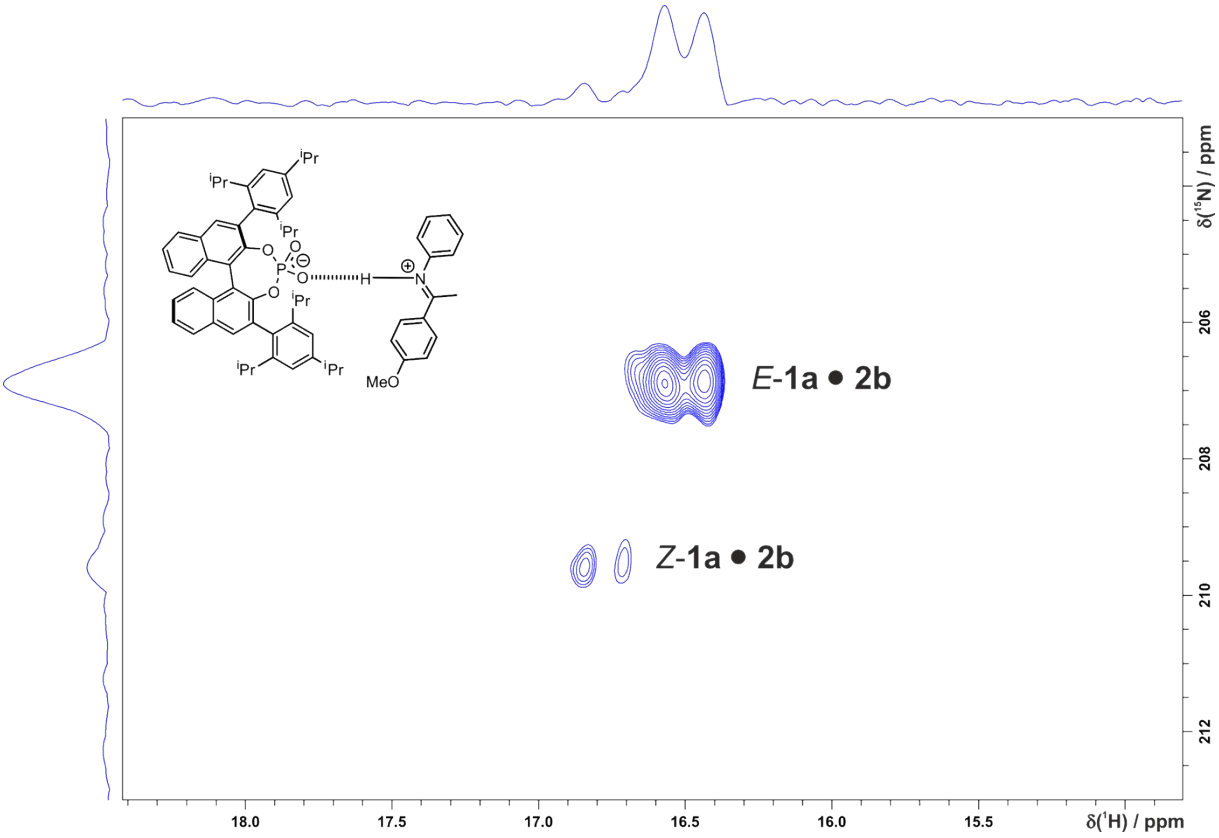

Figure S15: Low field section of the ^{1}H, ^{15}N-SOFAST-CLIP-HMQC acquired for **1a•2b** at 180 K. Further information: NS = 1024, (2 TD, 1 TD) = (4096, 32), AQ = 114 ms, O1P = 16.55, O3P = 208, CNST4 = 82. Acquired in 80 min.

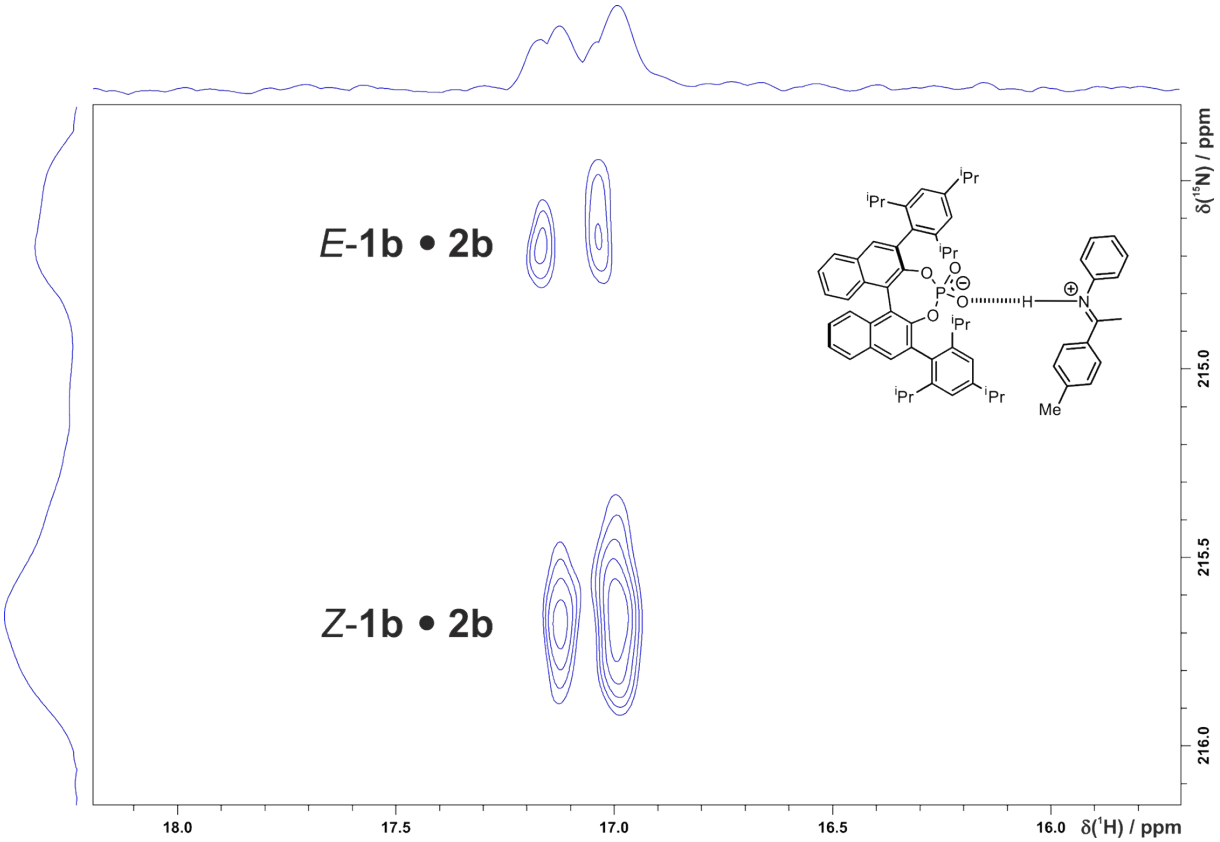

Figure S16: Low field section of the ^{1}H, ^{15}N-SOFAST-CLIP-HMQC acquired for **1b•2b** at 180 K. Further information: NS = 1024, (2 TD, 1 TD) = (2048, 32), AQ = 114 ms, O1P = 17.00, O3P = 214.9, CNST4 = 79. Acquired in 141 min.

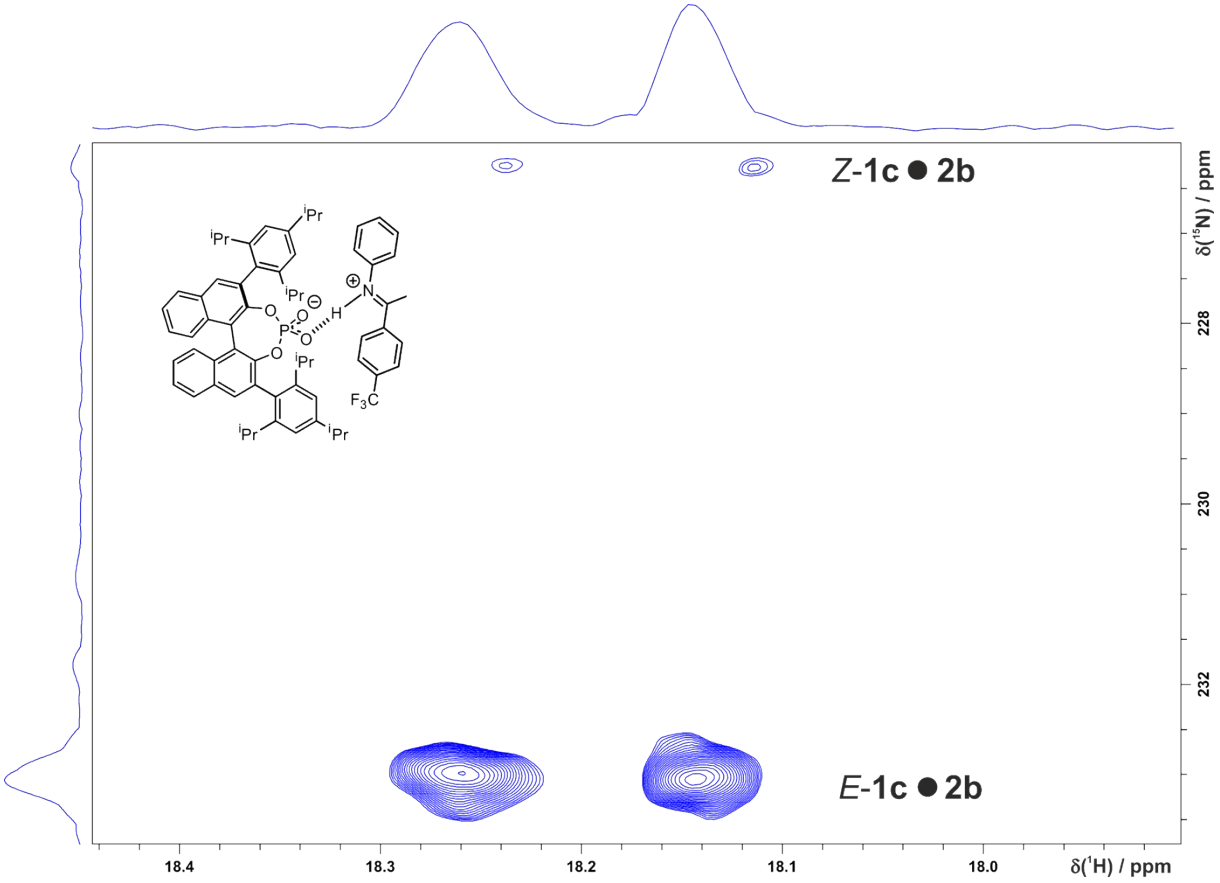

Figure S17: Low field section of the ^{1}H, ^{15}N-SOFAST-CLIP-HMQC acquired for **1c•2b** at 180 K. Further information: NS = 2048, (2 TD, 1 TD) = (4096, 32), AQ = 114 ms, O1P = 18.20, O3P = 231.5, CNST4 = 71. Acquired in 328 min.

S5.3 Binary Complexes of imines formed with acid 3 (HBF_4)

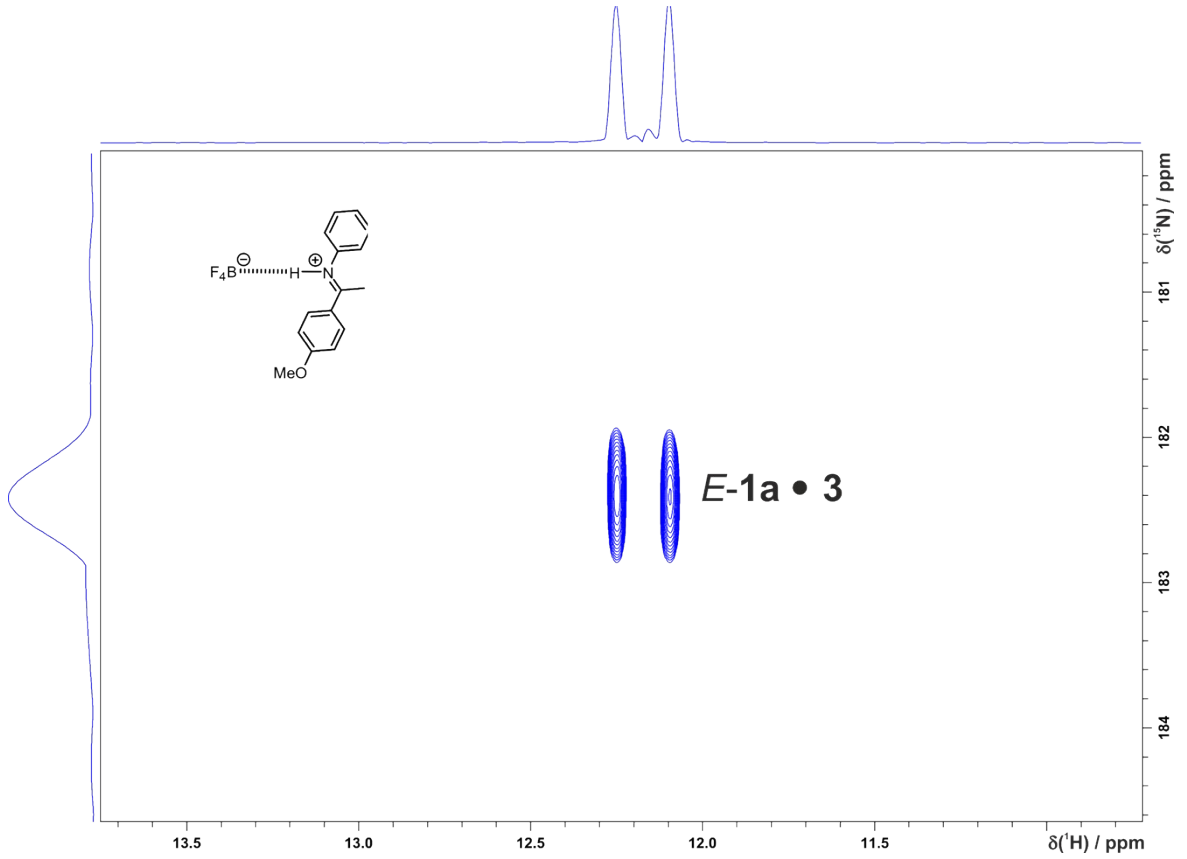

Figure S18: Low field section of the ^{1}H, ^{15}N-SOFAST-CLIP-HMQC acquired for **1a•3** at 180 K. Further information: NS = 2048, (2 TD, 1 TD) = (2048, 32), AQ = 114 ms, O1P = 17.28, O3P = 185.00, CNST4 = 93. Acquired in 339 min.

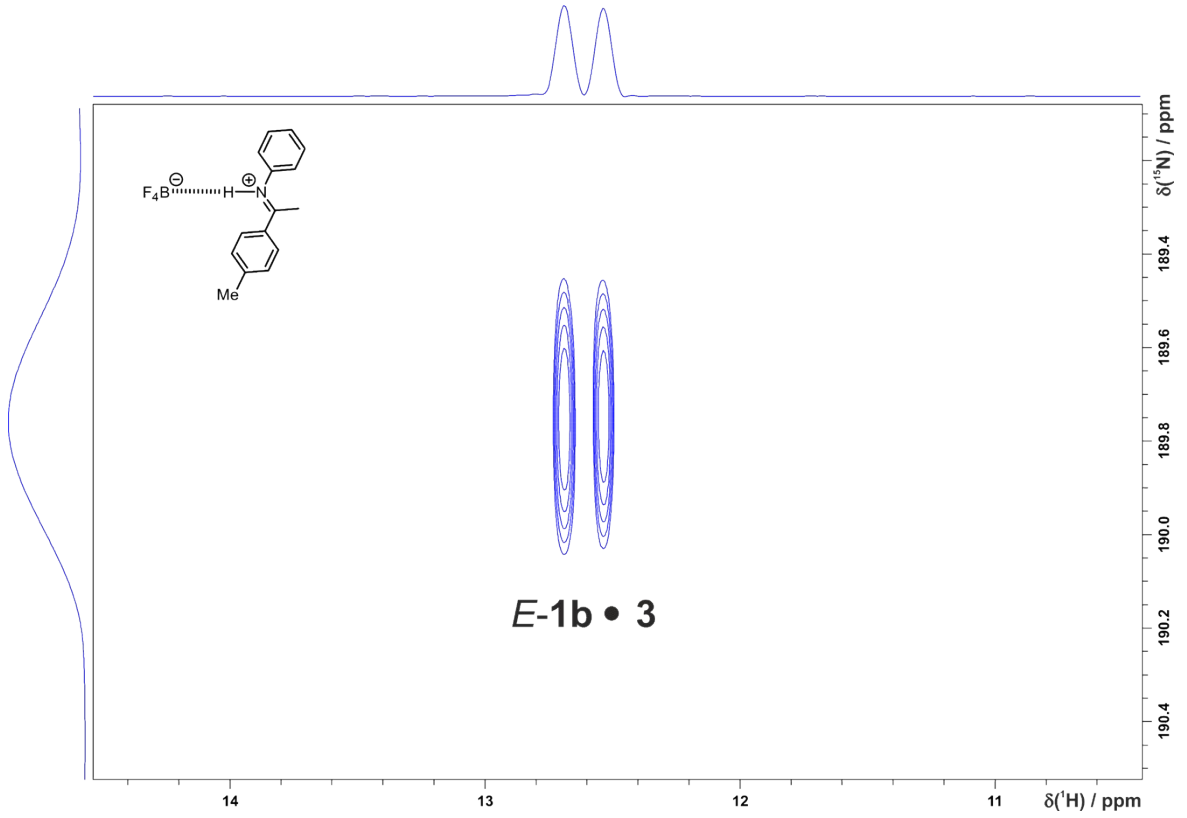

Figure S19 Low field section of the ^{1}H, ^{15}N-SOFAST-CLIP-HMQC acquired for **1b•3** at 180 K. Further information: NS = 4096, (2 TD, 1 TD) = (2048, 16), AQ = 57 ms, O1P = 12.68, O3P = 192.40, CNST4 = 92. Acquired in 258 min

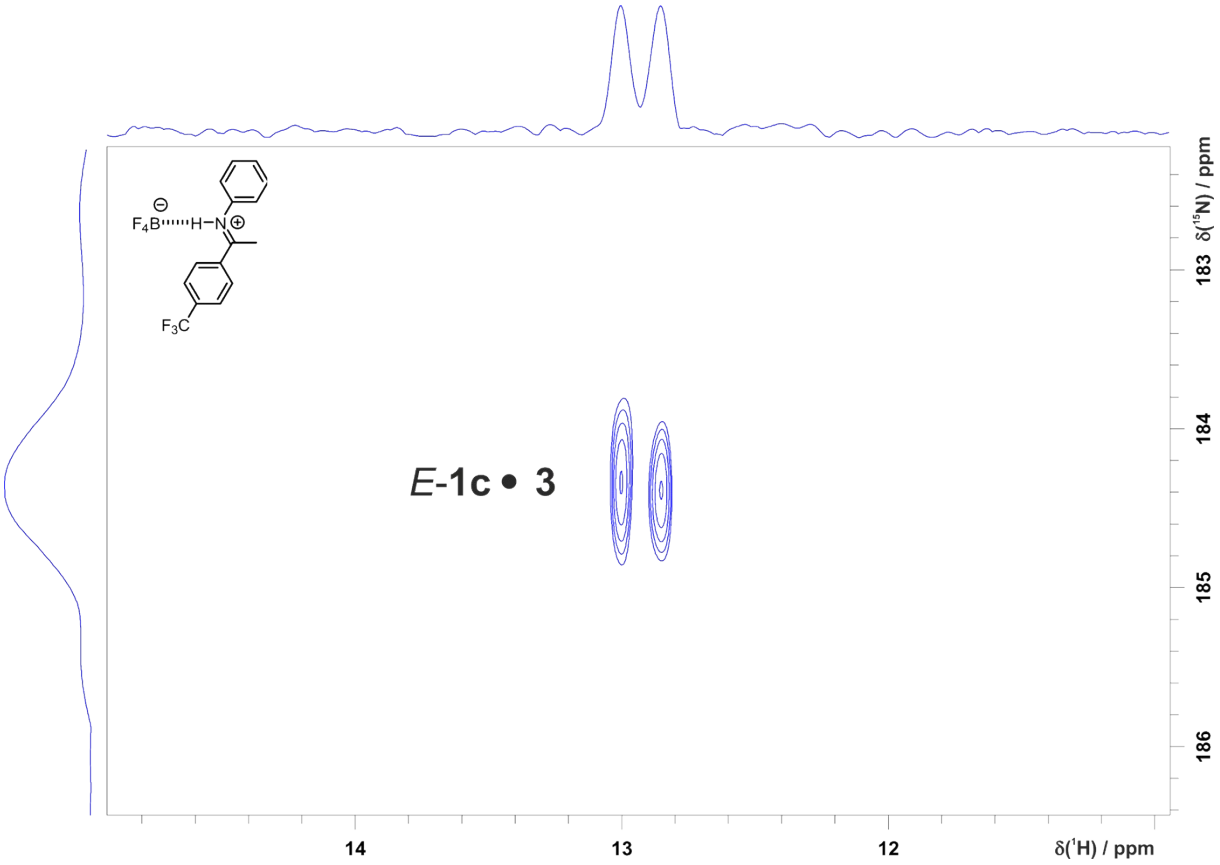

Figure S20: Low field section of the ^{1}H, ^{15}N-SOFAST-CLIP-HMQC acquired for **1c•3** at 180 K. Further information: NS = 64, (2 TD, 1 TD) = (8k, 32), AQ = 228 ms, O1P = 13.00, O3P = 183, CNST4 = 92. Acquired in 254 min.

S6 SOFAST-HMBC Spectrum and Parameters

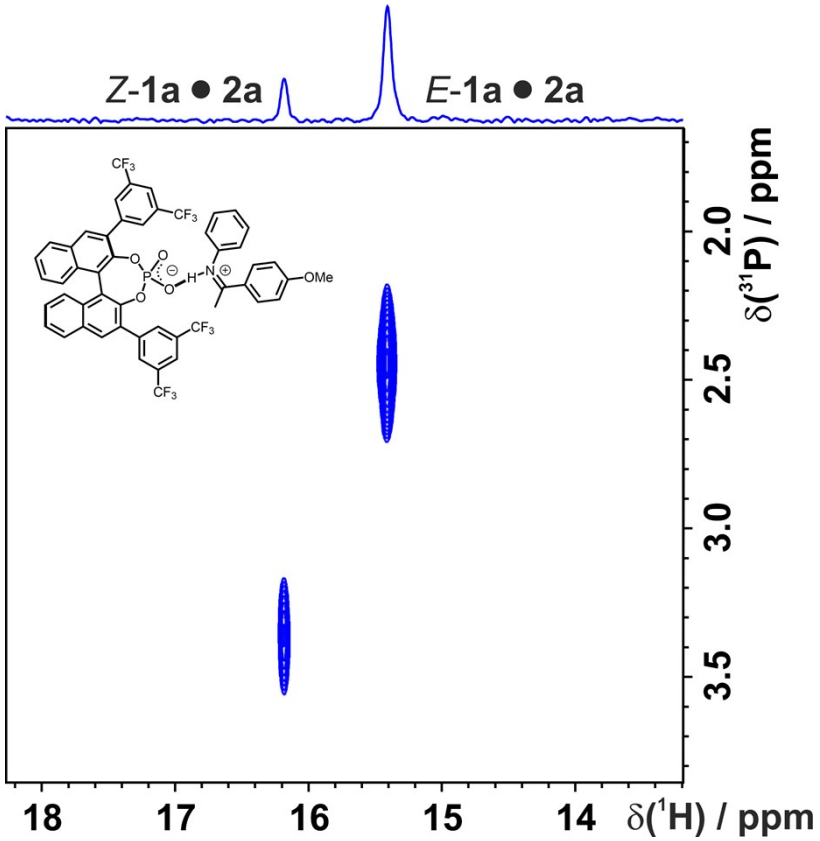

Figure S21: Low field section of the ^{1}H, ^{15}N-SOFAST-HMBC acquired for **1a•2a** at 180 K. Further information: NS = 256, (2 TD, 1 TD) = (4k, 32), AQ = 114 ms, O1P = 15.79, O2P = 2.85, CNST13 = 50. Acquired in 30 min.

S7 Steiner-Limbach Theory

The Steiner-Limbach curve links several NMR parameters which allows the characterization and the determination of the relative strength of hydrogen bonds. If the chemical shifts correlate with the Steiner-Limbach curve this indicates that the energy potential curve of the hydrogen bonds are described best by a single-well potential. A deviation from the correlation hints at a double-well potential. For typical CPAs single-well potentials were observed with the data points following the parabolic shape of the Steiner-Limbach curve. In contrast, stronger acids, such as *N*-triflyl phosphoramides (NTPAs), are deviating from the parabolic shape and follow a linear correlation indicating a double-well potential. HBF_4 is known to be an even stronger acid than the NTPAs, which is corroborated by the relative position on the Steiner-Limbach curve.[11] Therefore, the linear trend (Figure S22) resulting from the data points with HBF_4 agrees with the expected double-well potential.

The parametrized curve is defined by Eq. 1 and Eq. 2.

$$\delta(O\underline{H}N) = \delta(O\underline{H})^0\, p_{OH}^H + \delta(\underline{H}N)^0\, p_{HN}^H + 4\,\delta(O\underline{H}N)^*\, p_{OH}^H\, p_{HN}^H \quad \text{(Eq. 1)}$$

$$\delta(OH\underline{N})_{ref} = \delta(\underline{N})^0\, p_{OH}^H + \delta(H\underline{N})^0\, p_{HN}^H + 4\,\delta(OH\underline{N})^*\, p_{OH}^H\, p_{HN}^H \quad \text{(Eq. 2)}$$

The chemical shift of the hydrogen bond proton is denoted as $\delta(O\underline{H}N)$, whereas it is common to reference the measured chemical shift of the corresponding nitrogen $\delta(OH\underline{N})$ to the ^{15}N chemical shift of 1-(3,5-bis(trifluoromethyl)phenyl)-*N*-phenylethan-1-imine to obtain $\delta(OH\underline{N})_{ref}$. If done so $\delta(\underline{N})^0$ can be set to 0. $\delta(\underline{H}N)^0$ and $\delta(H\underline{N})^0$ designate the ^{1}H, respectively the ^{15}N chemical shift of the completely protonated imine. $\delta(O\underline{H})^0$ refers to the chemical shift of the free phosphoric acid. The parameters $\delta(O\underline{H}N)^*$ and $\delta(OH\underline{N})^*$ are correction factors to account for the asymmetry of the investigated complexes compared to symmetric XHX complexes. Finally, p_{OH}^H and p_{HN}^H refer to the corrected valence bond orders of the OH and NH bonds, respectively, whereby they need fulfil Eq. 3-5.[S12–15]

$$p_{OH}^H = p_{OH} - c^H\,(p_{OH}\,p_{HN})^f\,(p_{OH} - p_{HN}) - d^H\,(p_{OH}\,p_{HN})^g \quad \text{(Eq. 3)}$$

$$p_{HN}^H = p_{HN} + c^H\,(p_{OH}\,p_{HN})^f\,(p_{OH} - p_{HN}) - d^H\,(p_{OH}\,p_{HN})^g \quad \text{(Eq. 4)}$$

$$p_{ON}^H + p_{HN}^H = 1 \quad \text{(Eq. 5)}$$

In Eq. 3-4 p_{OH} and p_{HN} are the valence bond order before considering the zero anharmonic vibrations of the hydrogen atom within the hydrogen bond. The fitting parameters d^H, c^H, f and g have been determined in our previous work. For all required parameters to establish the Steiner-Limbach curve refer to Figure S22. All parameters have been adopted from literature.[S1]

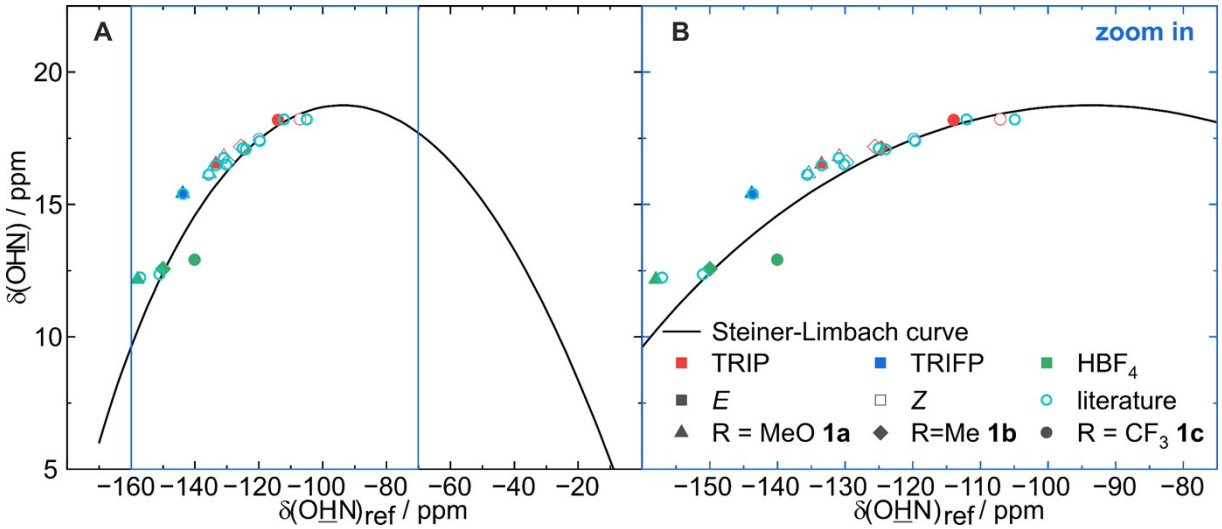

Figure S22: Steiner-Limbach curve showing literature data (turquoise, open circles) and measured chemical shifts using ^{1}H, ^{15}N-SOFAST-HMQC. For the complex *E*-**1c•3** reference point was available in literature. Parameters used to establish the Steiner-Limbach curve: δ(N)° = 0 ppm, δ(HN)° = -170 ppm, δ(OHN)* = -6 ppm, δ(OH)° = 2 ppm, δ(HN)° = 6 ppm, δ(OHN)° = 16 ppm, f = 8, g = 2, c^{H} = 360 and d^{H} = 0.3.[S1].

S8 ^{1}H-NOESY and ^{1}H-ROESY spectra of 1a•2a

Before applying SOFAST techniques, we strongly advise to acquire both ^{1}H-NOESY and ^{1}H-ROESY spectra. First, this helps to discriminate between molecules which fall into the slow- or fast-tumbling regime. For slow-tumbling compounds cross-peaks originating from NOE contacts have the same sign as the diagonal peaks in the ^{1}H-NOESY spectrum. However, this holds also true for cross-peaks originating from chemical exchange. Herein, the ^{1}H-ROESY spectrum helps discriminate between chemical exchange and NOE for all tumbling regimes. Second, a high number of NOE contacts hints at an accelerated relaxation upon selective treatment compared to hard pulse experiments. The relevance of these factors originates in the cross-relaxation σ of the investigated hydrogen bond. In the slow-tumbling regime the cross-relaxation σ becomes negative. Upon selective excitation, the effect of a negative cross-relaxation σ can be visualised by a magnetization flowing away from the excited hydrogen bond proton towards the NOE contact partners. This accelerates the longitudinal relaxation process. In contrast, a positive cross-relaxation σ increases the longitudinal relaxation upon selective excitation. The fast tumbling of low molecular substances, which is accompanied by positive or near-zero cross-relaxation, explains the limited applicability of SOFAST techniques. In conclusion, the sign of the cross-relaxation is key to determine whether selective pulses increase or reduce the T_1 relaxation time of the excited protons. For further explanations see reference.[S16]

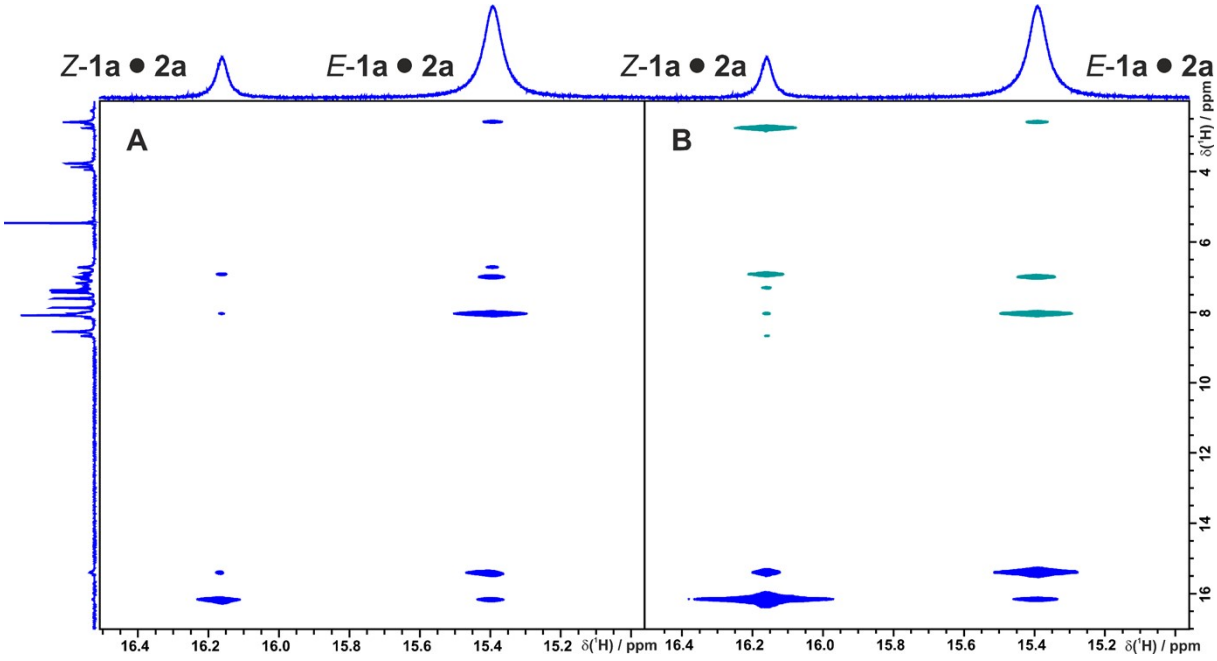

Figure S23: **A** ^{1}H-NOESY and **B** ^{1}H-ROESY acquired for **1a•2a** at 180 K. (positive sign: blue, negative peaks: green).

S9 Inversion Recovery Experiments

S9.1 Theory

As commonly known, once spins have been excited, they are relaxing back to thermal equilibrium. Mathematically, the relaxation process is described by means of lifetimes, i.e. the amount of time required to get from the maximal magnetization M_z^0 to about 37 % of M_z^0. Two different lifetimes are used to describe relaxation in NMR spectroscopy. (I) The longitudinal relaxation, referred to as T_1, describes the stimulated relaxation process which occurs by depopulating β and populating the α spins. (II) The transversal relaxation time T_2 describes the dephasing process of the spin ensemble in the transversal plane. In the following, we will only focus on the longitudinal relaxation time T_1. In diamagnetic samples, the main relaxation pathway contributing to T_1 are dipolar-dipolar interactions between ^{1}H spins. For the quantification of longitudinal relaxation time T_1 time inversion experiments are performed. In this one, first an inversion pulse is performed then after a delay τ, which will be incremented, a 90° pulse is applied. By serial integration and normalization to the last integral, inversion recovery plots, as shown below, are obtained. The magnetization decay is mathematically described by Eq. 6, in the following referred to as ExpDec1.

$$M_z(t) = M_z^0\left(1 - 2\exp\left(\frac{\tau}{T_1}\right)\right) \qquad \text{(Eq. 6)}$$

In contrast to the broadband excitation, this equation fails to describe the longitudinal relaxation when spins are excited selectively. This becomes visible by contemplating the recovery inversion plots below. A full mathematical description would require considering multi-spin system. However, a detailed quantitative analysis would go beyond the scope of this investigation. For the qualitative description of the selective longitudinal relaxation, the mathematical description of a two-spin system, which has been thoroughly discussed in literature, has been employed. Considering two spins I_1 and I_2 with initial magnetization given by $M_{1z} = M_z^0$ and $M_{2z} = -M_z^0$, i.e. I_2 has been inverted selectively. Solving the Solomon equations for a two-spin system describes how the longitudinal magnetization of spin I_2 will evolve.

$$M_{2z}(t) = M_z^0 \cdot \left(1 - e^{-(\rho+\sigma)\tau} - e^{-(\rho-\sigma)\tau}\right) \qquad \text{(Eq. 7)}$$

In Eq. 7, referred to as selT1, the rate constants ρ and σ describe the auto-relaxation and cross-relaxation of spin I_2, respectively. The auto-relaxation ρ depends on the spin's deviation from thermal equilibrium, whereas the latter is influenced by the deviation from thermal equilibrium of the second spin I_1. The cross-relaxation is the crucial parameter, responsible for the different relaxation upon selective excitation for slow or fast tumbling molecules. Only if the cross-relaxation is negative SOFAST-HMQC is advantageous over hard pulse HMQC pulse sequences. The two discussed rate constants can be obtained by fitting the inversion recovery plot two Eq. 7. Though, obviously the longitudinal relaxation can no longer be characterized with one relaxation time only even for this simplified model. However, by recurring to the original definition of a lifetime, the "selective longitudinal relaxation time" T_1^{sel} has been defined by Eq. 8 for this paper. Eq. 8 was iteratively solved to get a value for T_1^{sel}.

$$1 - e^{-(\rho+\sigma)T_1^{sel}} - e^{-(\rho-\sigma)T_1^{sel}} = \frac{1}{e} \qquad \text{(Eq. 8)}$$

S9.2 Inversion recovery experiments of the hydrogen bond proton in 99.5 % DCM-d_2

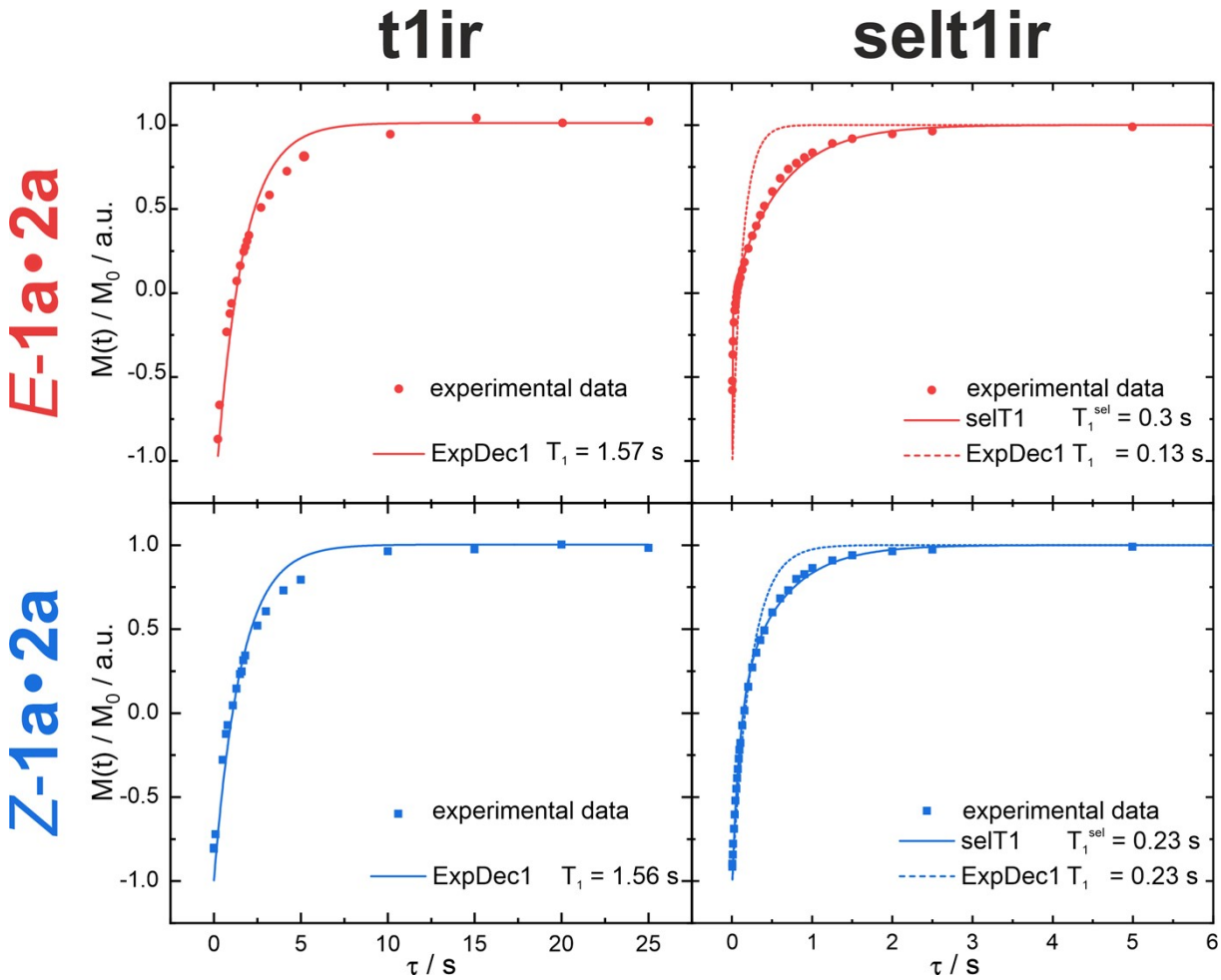

Figure S24: Inversion recovery plots performed on the hydrogen bond of *E*- (red) and *Z*-**1a•2a** (blue) in DCM-d_2 (99.5 %) at 180 K. Broadband (t1ir) and selective (selt1ir) inversion recovery experiments performed as described in section S9.1

S9.3 Inversion recovery experiments of the hydrogen bond proton in 10 % DCM-d_2

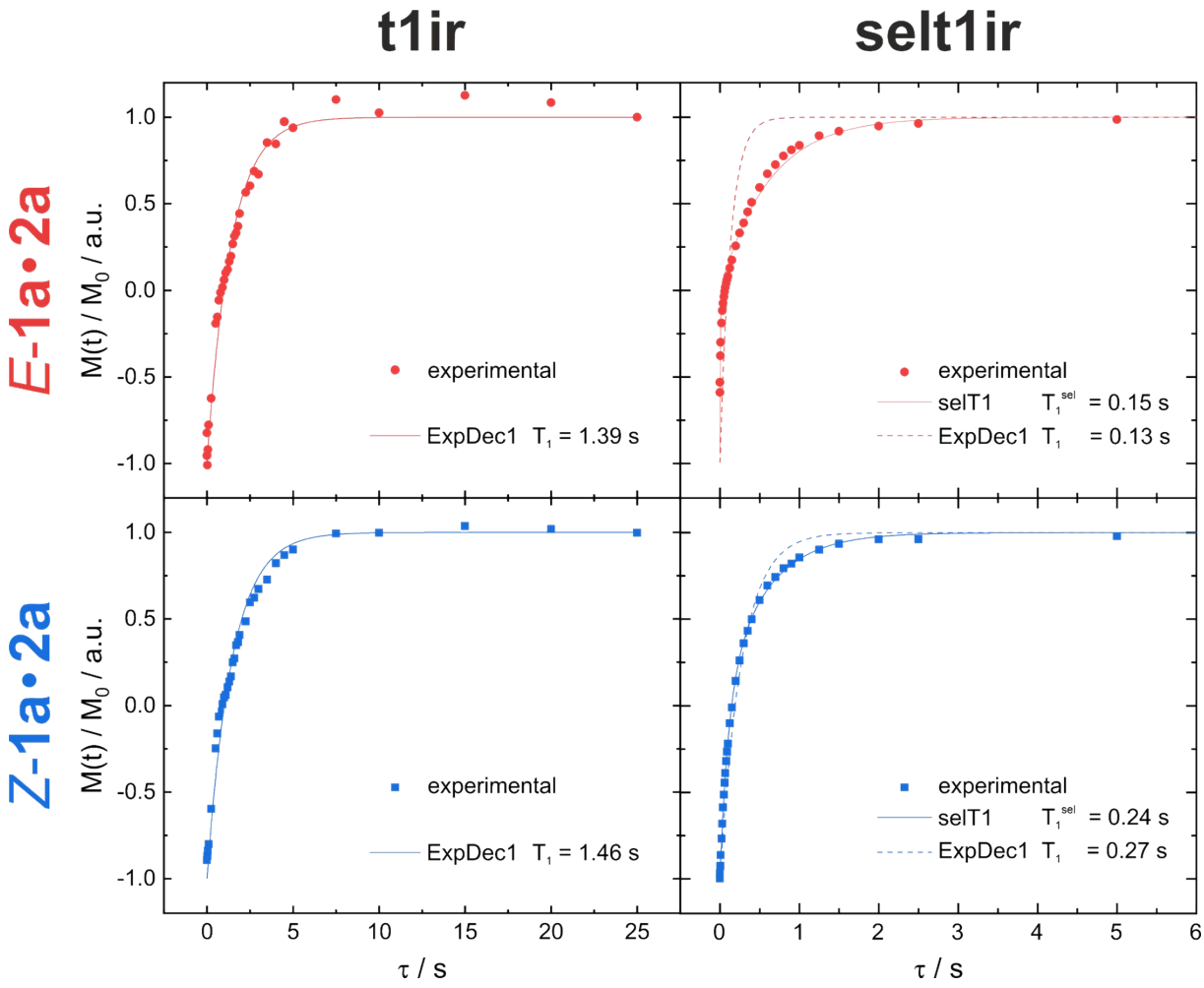

Figure S25 Inversion recovery plots performed on the hydrogen bond proton of *E*- (red) and *Z*-**1a•2a** (blue) in 10 % deuterated DCM at 180 K. Broadband (t1ir) and selective (selt1ir) inversion recovery experiments performed as described in section S9.1

S9.4 Inversion recovery experiments of the methyl protons in 99.5 % DCM-d_2

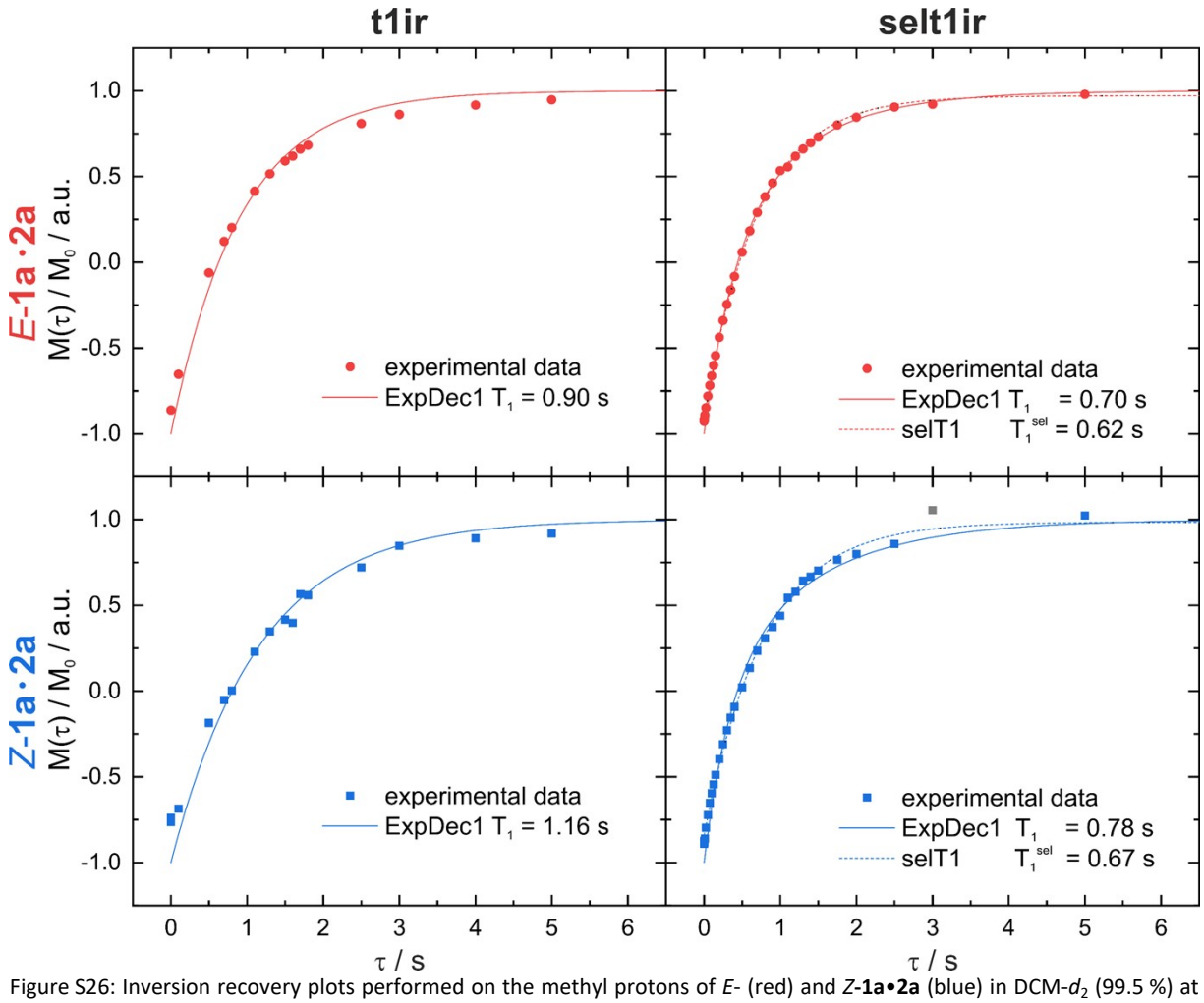

Figure S26: Inversion recovery plots performed on the methyl protons of *E*- (red) and *Z*-**1a•2a** (blue) in DCM-d_2 (99.5 %) at 180 K. Broadband (t1ir) and selective (selt1ir) inversion recovery experiments performed as described in section S9.1 Grey point marks an outliner which has not been considered for the fits.

S9.5 Inversion recovery experiments of the methyl protons in 10 % DCM-d_2

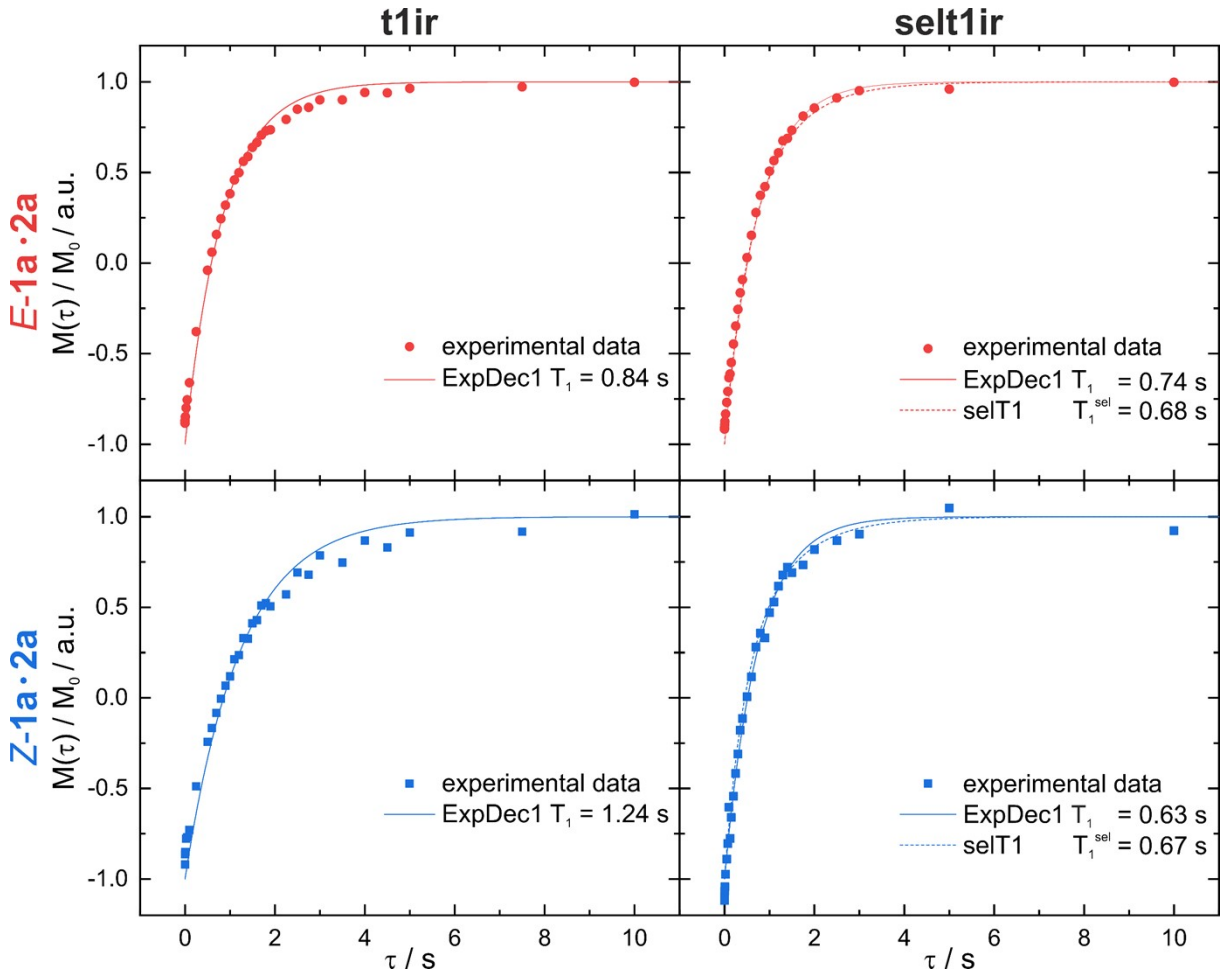

Figure S27: Inversion recovery plots performed on the methyl protons of *E*- (red) and *Z*-**1a•2a** (blue) in DCM-d_2 (10 %) at 180 K. Broadband (t1ir) and selective (selt1ir) inversion recovery experiments performed as described in section S9.1

S9.6 Inversion recovery experiments of the methoxy protons in 99.5 % DCM-d_2

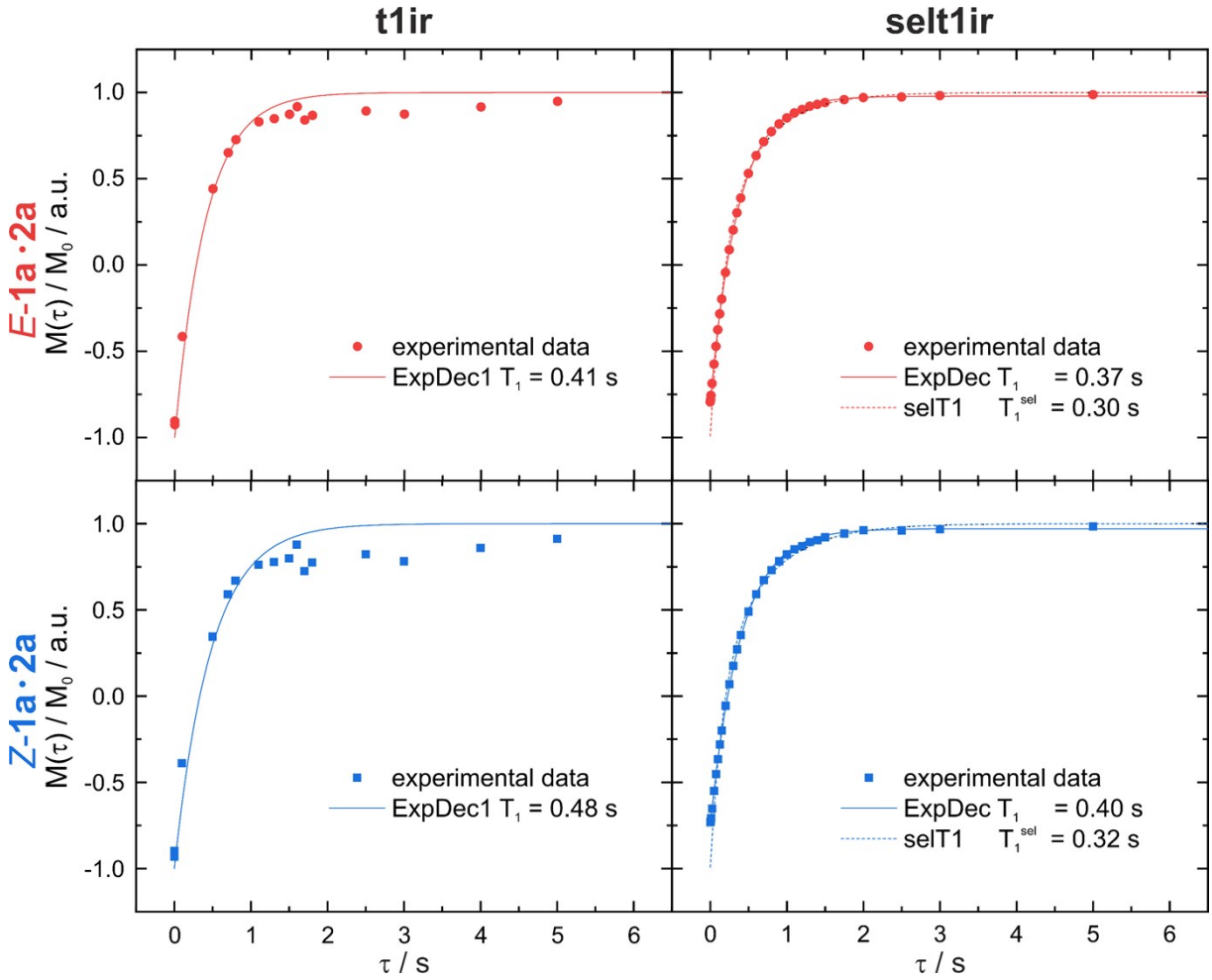

Figure S28: Inversion recovery plots performed on the methoxy protons of *E*- (red) and *Z*-**1a•2a** (blue) in DCM-d_2 (99.5 %) at 180 K. Broadband (t1ir) and selective (selt1ir) inversion recovery experiments performed as described in section S9.1

S9.7 Inversion recovery experiments of the methoxy protons in 10 % DCM-d_2

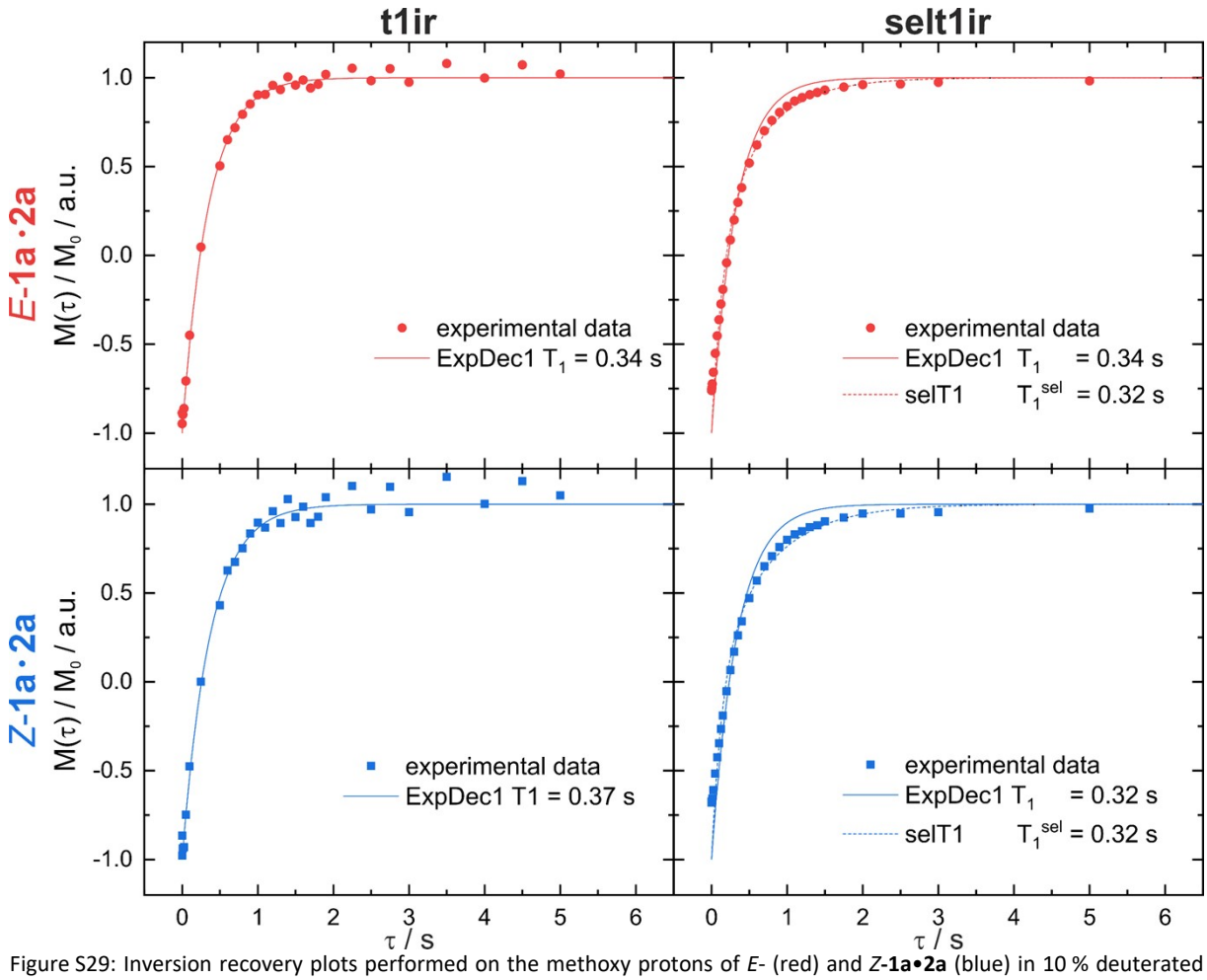

Figure S29: Inversion recovery plots performed on the methoxy protons of *E*- (red) and *Z*-**1a•2a** (blue) in 10 % deuterated DCM at 180 K. Broadband (t1ir) and selective (selt1ir) inversion recovery experiments performed as described in section S9.1

S9.8 Fitting values

Table S1: Fitted longitudinal relaxation time T_1 with fitting error of the hydrogen bond proton H(N), the methoxy- and methyl group of 1a•2a obtained from fitting the inversion recovery data acquired with a broadband pulse with Eq. 6. The data were acquired at 180 K in DCM-d_2 (99.5 % and 10 %).

Assignment	Group	T_1 / s	
		in 99.5 % DCM-d_2	in 10 % DCM-d_2
E-**1a•2a**	H(N)	1.57 ± 0.08	1.39 ± 0.04
	MeO	0.41 ± 0.03	0.34 ± 0.01
	Me	0.90 ± 0.03	0.84 ± 0.02
Z-**1a•2a**	H(N)	1.56 ± 0.08	1.46 ± 0.04
	MeO	0.48 ± 0.05	0.37 ± 0.02
	Me	1.16 ± 0.06	1.24 ± 0.04

Table S2: Fitted rate constants ρ and σ with fitting error of the hydrogen bond proton H(N), the methoxy- and methyl group of 1a•2a obtained from fitting the inversion recovery data acquired with a selective pulse with Eq. 7. T_1^{sel} was obtained by solving Eq. 8 with the obtained values for ρ and σ. The data were acquired at 180 K in 99.5 % DCM-d_2.

Assignment	Group	ρ / Hz	σ / Hz	T_1^{sel} / s
E-**1a•2a**	H(N)	90 ± 19	-89 ± 19	0.3[a]
	MeO	3.49 ± 0.09	-0.9 ± 0.3	0.30
	Me	1.9 ± 0.1	-1.0 ± 0.2	0.62
Z-**1a•2a**	H(N)	6.6 ± 0.2	-4.8 ± 0.3	0.23
	MeO	4.0 ± 0.4	-2.4 ± 0.4	0.32
	Me	1.8 ± 0.1	-1.0 ± 0.2	0.67

a Faulty due to the high fitting errors of ρ and σ.

Table S3: Fitted rate constants ρ and σ with fitting error of the hydrogen bond proton H(N), the methoxy- and methyl group of 1a•2a obtained from fitting the inversion recovery data acquired with a selective pulse with Eq. 7. T_1^{sel} was obtained by solving Eq. 8 with the obtained values for ρ and σ. The data were acquired at 180 K in 10 % DCM-d_2.

Assignment	Group	ρ / Hz	σ / Hz	T_1^{sel} / s
E-**1a•2a**	H(N)	89 ± 19	-87 ± 19	0.15[a]
	MeO	4.0 ± 0.4	-2.4 ± 0.4	0.32
	Me	1.52 ± 0.01	-0.36 ± 0.03	0.68
Z-**1a•2a**	H(N)	5.73 ± 0.08	-3.9 ± 0.09	0.24
	MeO	4.3 ± 0.5	-2.9 ± 0.6	0.32
	Me	1.8 ± 0.1	-1.0 ± 0.2	0.67

a Faulty due to the high fitting errors of ρ and σ.

S10 Sensitivity Enhancement

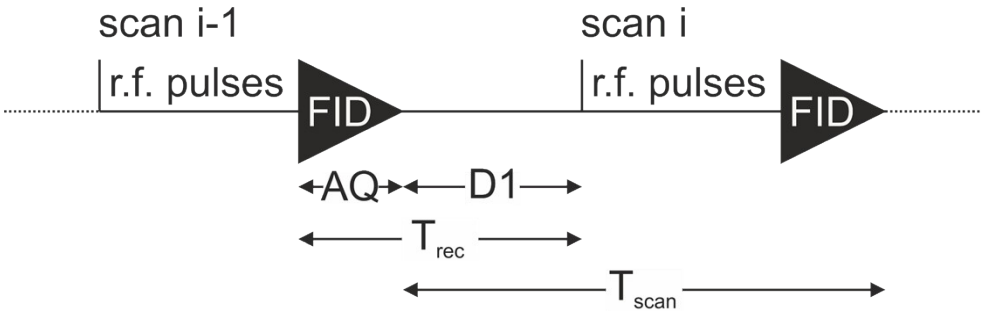

Figure S30: General scheme for time-domain NMR experiments illustrating the relevant delays for the evaluation of sensitivity enhancement curves.

S10.1 Acquisition and evaluation of the data

For the acquisition of the data shown in Figure 4B, 24 experiments were acquired for each data set. All delays are illustrated in Figure S30. The total amount of time required for one experiment was set to 66 s. The acquisition time AQ amounted to 57 ms and the pulse sequence took 7.2 ms. While the number of scans were decreased for each experiment, starting from 512 to 16, the recovery delay D1 was increased from 30 ms to 1.97 s. For the evaluation of the data, a serial integration over all data sets has been performed. To account for the different number of scans, the integrals have been normalized by the square root of the number of scans.

S10.2 Theory

For the binary complex **1a•2a** the highest sensitivity gain was achieved for an excitation angle of 115°. This agrees with literature data[S3] as all sensitivity enhancement curves shown in Figure 4B follow Eq. 9.[17]

$$\left(\frac{S}{N}\right) \propto \frac{\left(1 - \exp\left(-\frac{T_{rec}}{T_1}\right)\right) \cdot \sin\beta}{1 - \exp\left(-\frac{T_{rec}}{T_1}\right)\cos\beta} \cdot \sqrt{n\,T_{scan}}^{-1} \qquad \text{(Eq. 9)}$$

S11 Signal to Noise

To measure the signal to noise ratio (S/N) obtained when using the SOFAST-HMQC to a regular HMQC pulse sequence, i.e. using hard pulses, the pulse sequence *sfhmqcf3gpph* was adapted accordingly. Both spectra shown in Figure S31 and Figure S32 were recorded using 256 scans and 32 increments in the indirect dimension. The SOFAST-HMQC was recorded using a relaxation delay D1 of 100 ms, while for the regular HMQC 1 s was used. The acquisition of the SOFAST-HMQC required 30 min. The measurement of the regular HMQC took 2 h 40 min. For the former a S/N of 18 was obtained, while the regular HMQC led to a S/N of 14.

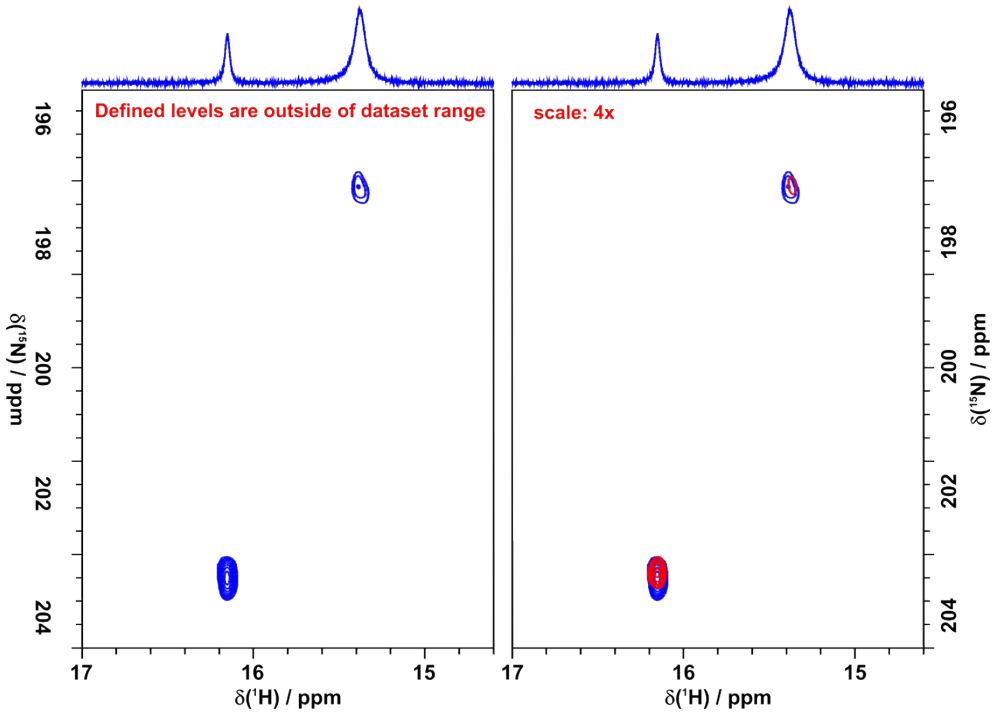

Figure S31: Low field section of the ^{1}H, ^{15}N-SOFAST-HMQC (blue) and regular ^{1}H, ^{15}N-HMQC (red) acquired for **1a•2a** at 180 K. Further information for the ^{1}H, ^{15}N-SOFAST-HMQC: NS = 256, (2 TD, 1 TD) = (2048, 32), AQ = 57 ms, O1P = 15.79, O3P = 200, CNST4 = 85, D1 = 100 ms. Acquired in 30 min. Further information for the ^{1}H, ^{15}N-HMQC: NS = 256, (2 TD, 1 TD) = (4096, 32), AQ = 114 ms, O1P = 15.79, O3P = 200, CNST4 = 85, D1 = 1s. Acquired in 2 h 40min.

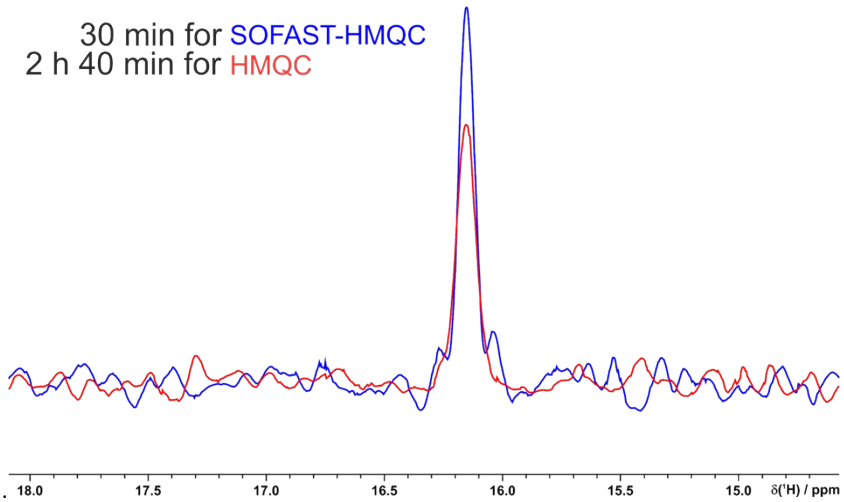

Figure S32: For the ^{1}H, ^{15}N-SOFAST-HMQC (blue) and the regular ^{1}H, ^{15}N-HMQC (red) shown in Figure S31 the row with the corresponding maximal intensity of the *Z*-**1a•2a** peak has been extracted. A S/N of 18 has been obtained for the SOFAST-HMQC. For the regular HMQC a S/N of 14 was obtained. For further information refer to Figure S31.

S12 Additional complex: DIPEA•2b

The prerequisite for this method is a lifetime of the hydrogen bond long enough to allow coherence transfer. Long enough lifetimes can be achieved via cooperative hydrogen bond networks, e.g., in biomolecules, such as proteins, or via strong hydrogen bonds. How an extension of the lifetimes is achieved in the individual system does not matter. Typical conditions for small molecules are charge-assisted strong hydrogen bonds in apolar organic solvents as used in our benchmark system. Additionally, exchange processes can be reduced by choosing accurate ratio of hydrogen bond donor to acceptor. In case the lifetime of the hydrogen bond is long enough, and the investigated system is in the slow-tumbling regime the SOFAST method is generally applicable.

To broaden our scope, we were curious whether the suggested method also applies to other structural motifs such as tertiary amines, e.g., *N*-ethyl-*N*-isopropylpropan-2-amine (DIPEA), in combination with a CPA, such as **2b**. For this we used a concentration of 50 mM and a DIPEA:**2b** ratio of 1:1 at 180 K. Both the ^{1}H-^{15}N decoupled SOFAST-HMQC, as well as the SOFAST-CLIP-HMQC were applicable to this system as shown in Figure S33.

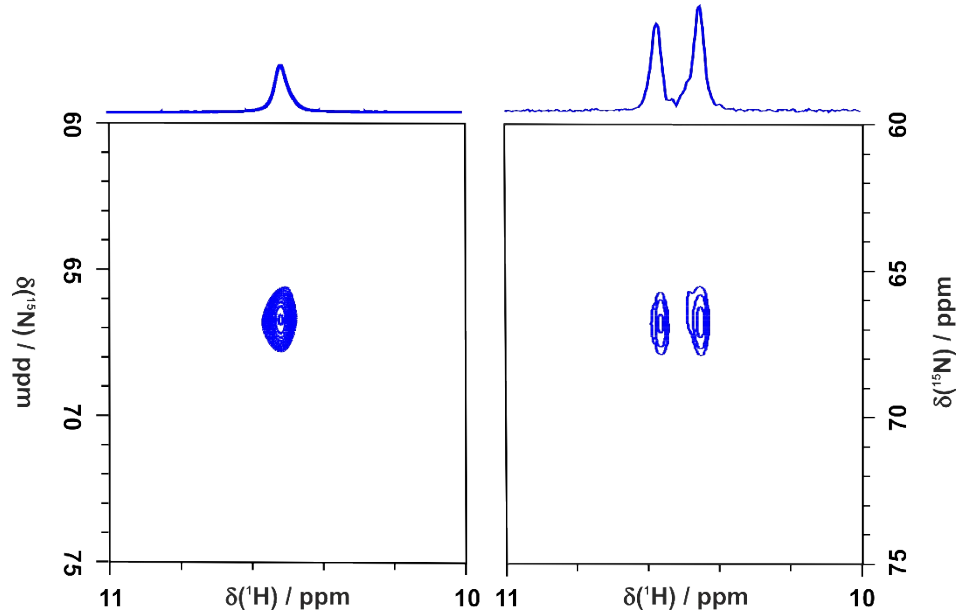

Figure S33: Low field section of the ^{1}H, ^{15}N-SOFAST-HMQC (blue) and regular ^{1}H, ^{15}N-HMQC (red) acquired for **DIPEA•2b** at 180 K. Further information for the ^{1}H, ^{15}N-SOFAST-HMQC: NS = 32, (2 TD, 1 TD) = (4k, 64), AQ = 114 ms, O1P = 10, O3P = 64.8, CNST4 = 72, D1 = 50 ms. Acquired in 7 min. Further information for the ^{1}H, ^{15}N-HMQC: NS = 64, (2 TD, 1 TD) = (8k, 64), AQ = 228 ms, O1P = 10, O3P = 64.8, CNST4 = 72, D1 = 50 ms. Acquired in 22 min.

References

1. K. Rothermel, M. Melikian, J. Hioe, J. Greindl, J. Gramüller, M. Žabka, N. Sorgenfrei, T. Hausler, F. Morana, R. M. Gschwind, *Chem Sci*, **2019***, 10*, 10025–10034.
2. N. Karschin, S. Krenek, D. Heyer, C. Griesinger, *Magn Reson Chem*, **2022***, 60*, 203–209.
3. P. Schanda, B. Brutscher, *J. Am. Chem. Soc.*, **2005***, 127*, 8014–8015.
4. P. Schanda, E. Kupce, B. Brutscher, *J Biomol NMR*, **2005***, 33*, 199–211.
5. A. Shaka, P. Barker, R. Freeman, *Journal of Magnetic Resonance (1969)*, **1985***, 64*, 547–552.
6. H. Geen, R. Freeman, *Journal of Magnetic Resonance (1969)*, **1991***, 93*, 93–141.
7. E. Kupce, R. Freeman, *Journal of Magnetic Resonance, Series A*, **1993***, 102*, 122–126.
8. D. Marion, M. Ikura, R. Tschudin, A. Bax, *Journal of Magnetic Resonance (1969)*, **1989***, 85*, 393–399.
9. A. Altmayer-Henzien, V. Declerck, D. J. Aitken, E. Lescop, D. Merlet, J. Farjon, *Org Biomol Chem*, **2013***, 11*, 7611–7615.
10. T. H. Mareci, R. Freeman, *Journal of Magnetic Resonance (1969)*, **1982***, 48*, 158–163.
11. M. Hecht, P. Dullinger, W. Silva, D. Horinek, R. M. Gschwind, *Chem Sci*, **2024***, 15*, 9104–9111.
12. H.-H. Limbach, M. Pietrzak, S. Sharif, P. M. Tolstoy, I. G. Shenderovich, S. N. Smirnov, N. S. Golubev, G. S. Denisov, *Chemistry*, **2004***, 10*, 5195–5204.
13. S. Sharif, G. S. Denisov, M. D. Toney, H.-H. Limbach, *J. Am. Chem. Soc.*, **2007***, 129*, 6313–6327.
14. H. Benedict, I. G. Shenderovich, O. L. Malkina, V. G. Malkin, G. S. Denisov, N. S. Golubev, H.-H. Limbach, *J. Am. Chem. Soc.*, **2000***, 122*, 1979–1988.
15. H.-H. Limbach, M. Pietrzak, H. Benedict, P. M. Tolstoy, N. S. Golubev, G. S. Denisov, *Journal of Molecular Structure*, **2004***, 706*, 115–119.
16. P. Schanda. *Development and application of fast NMR methods for the study of protein structure and dynamics*. Université Joseph-Fourier, **2007**.
17. Ernst, R., Bodenhausen, G., Wokaus, A. *Principles of Nuclear Magnetic Resonance in One and Two Dimensions.* Oxford Science Publications , **1987**.